THE PENNSYLVANIA STATE UNIVERSITY
SCHREYER HONORS COLLEGE

DEPARTMENT OF CHEMISTRY

CONVERSION OF THIN FILM GERMANIUM TO GERMANIUM TELLURIDE AND PROBING THE CATALYTIC PROPERTIES OF NANOPARTICLE GOLD/IRON-OXIDE HETERODIMERS

MICHAEL SCHRENK
SPRING 2014

A thesis
submitted in partial fulfillment
of the requirements
for a baccalaureate degree
in Chemical Engineering
with honors in Chemistry

Reviewed and approved* by the following:

Raymond E. Schaak
Professor of Chemistry
Thesis Supervisor

Raymond L. Funk
Professor of Chemistry
Honors Adviser

* Signatures are on file in the Schreyer Honors College.

ABSTRACT

Germanium telluride is a prototype phase change material that exhibits appreciable physical property differences between its amorphous and crystalline phase. These differences are exploited in many technological applications to store information in media such as DVDs and Blu-ray discs. Moreover, phase change materials such as germanium telluride are being investigated for use as metamaterials to elicit extraordinary electromagnetic parameters. Herein I report a novel methodology for the conversion of 100 nm thin germanium films on a silicon support to germanium telluride via reaction with a trioctylphosphine-tellurium complex. The product was confirmed and characterized using powder x-ray diffraction. The facile chemical approach presented combines current nanofabrication capabilities with more complex phase change materials to serve as a basic foundation for future metamaterial endeavors.

Also reported within this thesis is the examination of the magnetically separable, heterogeneous nanoparticle catalyst Au-Fe_3O_4. The dumbbell-like Au-Fe_3O_4 nanostructure is synthesized and studied for its ability to catalyze organic alcohol oxidation. Catalytic experiment parameters were systematically altered to account for reaction temperature, time, substrate, and solvent polarity. Surface effects of possible ligand moieties present after synthesis are also explored. The Au-Fe_3O_4 nanoparticle was also deposited on a variety of supports in an effort to induce the formation of new active sites between the Au-Fe_3O_4/support interface junction. Characterization of products was carried out using a variety of assays including powder x-ray diffraction, transmission electron microscopy, and gas chromatography.

TABLE OF CONTENTS

LIST OF FIGURES

ACKNOWLEDGEMENTS

First, I would like to acknowledge and thank Professor Ray Schaak for the opportunity to conduct research in his laboratory over the years. I am especially indebted to him for hiring me at moment's notice to conduct research during the summer of 2012. He has been a tremendous support and very helpful since joining the group.

I would also like to thank my mentor Dr. Matthew Remy, for without his guidance this thesis would not have come to fruition. Dr. Remy proved an invaluable resource and showed unwavering patience when answering my countless questions. He taught me the fundamentals of benchtop chemistry research and challenged me to critically think. Our thought-provoking discussions helped push my projects in a meaningful direction. I also express my gratitude for his career advice outside the laboratory. I owe him a great deal for all his help.

Additionally, I would like to thank the graduate and postdoctoral students of the Schaak Lab who have all helped me at some point along this memorable journey and who created a welcoming environment when I was just beginning. I would also like to thank and acknowledge the Penn State Electrical Engineering Department for providing the thin film germanium slides.

Chapter 1

Conversion of Thin Film Germanium to Germanium Telluride

Introduction

Germanium telluride is a Ge-based chalcogenide alloy that acts as a prototype for phase change materials due to its simple composition and structure[1]. A phase change material is any material that exhibits at least two stable solid phases in which all properties of the material are essentially uniform. The solid phases consist of one or more crystalline phases and an amorphous phase.[2] There exist many appreciable physical property differences between the two phases, which are the result of differences in the structure.

GeTe is a polymorphic compound with two crystal structures. The first, with a crystallization temperature above 400 ^{O}C, has a rock-salt arrangement with two fcc sublattices.[3] However at lower temperatures and in the ground state, GeTe exhibits a rhombohedral trigonal structure obtained by stretching the rock-salt unit cell along the <111> direction and shifting the central atom.[2]

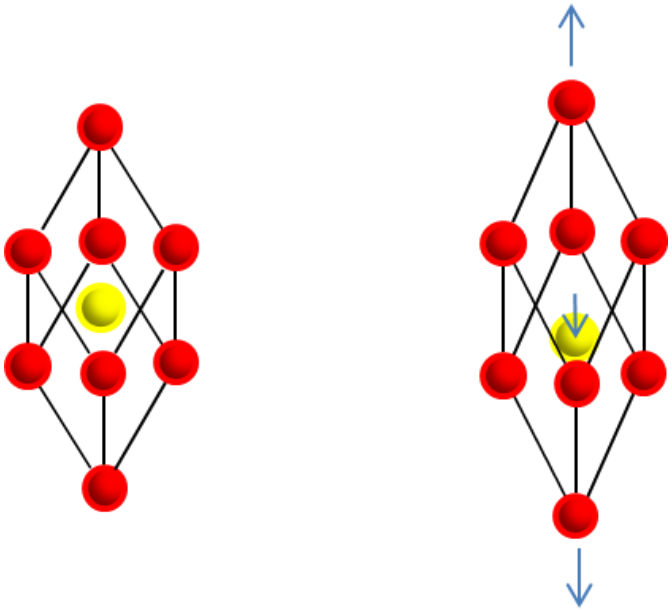

Figure 1. GeTe rock-salt structure (left) and trigonal structure (right); adapted from Reference 2

Conversely, the amorphous phase of GeTe does not have complete long range order or periodicity and therefore a definitive unit cell cannot be produced for the configuration of the atomic positions. Fortunately with the advent of improved computational power, modern molecular dynamic simulations show amorphous GeTe to have long-range ordering of Te atoms and alternating four-membered rings.[4]

There are also significant differences in the optical and electrical properties between the two phases that can be attributed to the very different atomic structures. The crystalline phase of GeTe has a much more distinctive, higher optical absorption intensity peak than amorphous GeTe exposed to the same wavelength conditions.[5] Furthermore, it has been shown that only alloys that crystallize in a rock-salt lattice such as GeTe display a sufficiently large optical contrast[6,7]. Concerning the electrical properties of phase change materials, it is generally accepted that the energy band gap of the amorphous

phase is larger than that of the crystalline phase.[2] GeTe is a ferroelectric narrow gap semiconductor and it has a crystalline (amorphous) band gap of about 0.1 (0.8) eV. The crystalline room-temperature resistivity is approximately 10^{-4} Ω•cm^2, many orders of magnitude less than its amorphous counterpart (10^3 Ω•cm^2)[8].

The phase change process is straightforward but not trivial. A short, high-intensity laser beam pulse known as the reset is used to locally heat the phase change material above its melting temperature. The alloy melt is then rapidly quenched and solidified into a disordered, amorphous state. The amorphous material can then be exposed to a long, intermediate-intensity laser known as the set that locally heats the phase change material above the crystallization temperature. The alloy is then allowed to cool and the atoms revert to the more energetically stable crystalline state[9].

There are two types of crystal nucleation. Homogenous nucleation is when the initial step begins inside the amorphous phase, while heterogeneous nucleation occurs between the amorphous phase and an outside boundary such as surfaces or interfaces with supports or impurities. It is important to note that the driving force behind the crystallization process is the difference in the Gibbs free energy between the amorphous and crystalline phase. One of the most useful properties of phase change materials such as GeTe is the kinetic time scale of the crystallization process. It has been demonstrated that the shortest recrystallization times are on the order of 400 ps for 1 μm spot diameter, while other industrially applicable phase change materials work on an average of the nanosecond time scale[10].

There are several qualities that phase change alloys must possess to find use in technological applications. High-speed phase transition, long thermal stability of the

amorphous and crystalline state, a large cycle number of reversible phase transitions, and the pronounced difference in optical and electrical properties between phases are all crucial to industrial relevance. Numerous phase change materials have one or more of these properties, but few possess all. Many of the phase change materials that are employed in technologies today are based on the GeTe-Sb_2Te_3 pseudobinary line of the Ge-Sb-Te phase diagram[11,12]. Another class of alloys used is Sb_2Te doped with In and Ag[9].

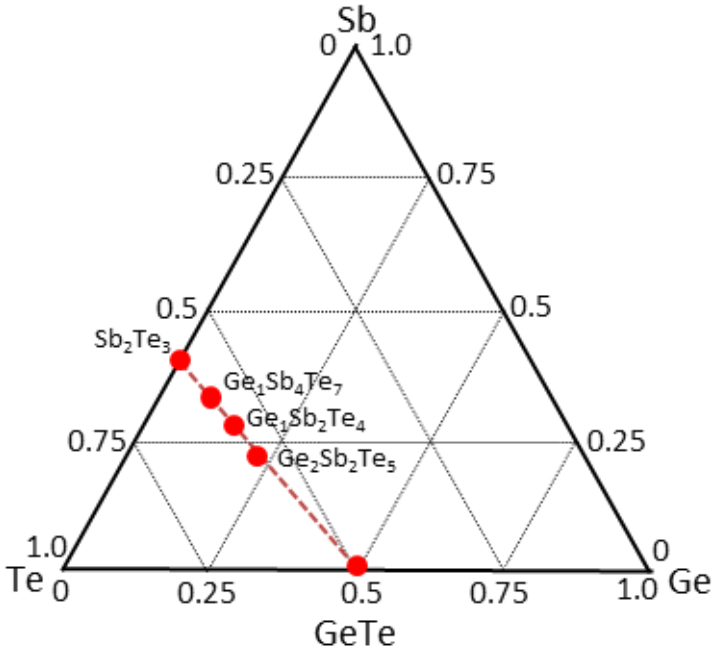

Figure 2. Ternary phase diagram of the Ge-Sb-Te system highlighting many successful industrial alloys; adapted from Reference 2

Phase change materials have contributed to the development of three generations of optical storage media systems including CDs, DVDs, and Blu-ray disks[9]. Initial writing of the media is done by writing amorphous bits onto a crystalline matrix of the disc that is then able to be read due to changes in reflectivity between the amorphous and

crystalline phase. Re-writing is also accomplished through the recrystallization of the amorphous bits. Another emerging technology utilizing phase change materials is phase change random access memory (PCRAM). This system rapidly switches between the amorphous and crystalline phases of phase changing materials using Joule heating, taking advantage of the change in resistivity of the two phases[2]. Phase change materials are also being explored as possible metamaterials.

Metamaterials are man-made materials that interact with electromagnetic waves in an anomalous fashion[13]. They are constructed on the sub-wavelength scale and present unusual yet useful functionalities. They have been pursued to elicit extraordinary electromagnetic parameters such as a negative refractive index, terahertz magnetism, and incredibly large chirality[14]. One of the most talked about applications of a metamaterial is the idea of invisibility or cloaking by changing the proportions of space for light so that it bends around an object of interest.[15] Recent publications have demonstrated an electromagnetic cloak at microwave frequencies[16], and negative refraction index at visible frequencies[17]. As research advances, phase change materials have also found a home in the metamaterial paradigm. $Ge_2Sb_2Te_5$ on the nanoscale thickness has been proposed for electro-optic switching[18], and a hybrid of phase changing VO_2 and a metamaterial has been reported as an electrically active memory function.[19]

In the following experiment, I demonstrate the ability to convert a thin nanoscale film of Ge deposited on a substrate into the phase changing material GeTe via a reaction with a trioctylphosphine-tellurium complex. This system serves as a very basic foundation for future metamaterial endeavors. Ge domains pre-engineered and strategically positioned on a substrate could, in principle, be converted to GeTe via the

same mechanism. These GeTe domains would be able to refract light into predetermined directions, such as to take a path around an object of interest. Moreover, because of the phase-changing nature of GeTe, the domains could be exposed to a heat source to transition from the crystalline phase to the amorphous phase. Due to the difference in optical properties between phases discussed earlier, the phase change could act as an on/off switch for directing light.

Germanium domains on silicon substrate supports are currently fabricated using top-down lithography combined with wet chemical etching methods[20]. These systems are generally well understood; however, the engineering ability to construct GeTe domains using similar techniques is not. The work presented here is a facile chemical approach that advantageously combines current nanofabrication capabilities with more complex phase change materials to produce heterogeneous structures with exciting potential applications.

Experimental

Materials.

The 100 and 200 nm germanium films/rods deposited on glass and silicon <100> substrates were obtained from the Penn State Electrical Engineering Department. The following chemicals were purchased and used without further purification. Tellurium powder (99.99%, - 325 mesh) and 1-Octadecene (tech. 90%) were purchased from Alfa Aesar. Trioctylphosphine (TOP, tech. 90%) was obtained from Aldrich. Iodine crystal (≥

99.8%) was purchased from Mallinckrodt. Sodium hydroxide (97%) was purchased from EMD. All reactions were carried out in a 20 mL septum cap vial using a standard Schlenk technique and were worked-up in air at room temperature.

Methods.

Conversion of Ge Film on Substrate to GeTe

A composite slide consisting of a thin (100-200 nm) Ge film on substrate was obtained. The slide was placed in a 20 mL septum cap vial and 10 mL deionized water were added to completely submerge the slide. 250 µL of 1 M NaOH were added to create a slightly basic solution. The vial was then sparged with argon and sonicated for 5 minutes to remove possible oxide buildup. The slide was removed from solution and washed quickly with deionized water followed by ethanol. The slide was then placed onto a support in a new 20 mL vial containing a magnetic stirrer. Vacuum was pulled for 5 minutes, the vial was subsequently backfilled with argon, and 3 mL of 1 M TOP-Te were added to submerge the slide. The solution was heated to 225^{o}C with moderate mixing for 45 minutes before allowing to cool to room temperature. The slide was then removed from solution, washed with hexanes followed by ethanol, and XRD analysis was performed.

Prior to the final successful experimental procedure, a number of trials were performed to systematically adjust the procedure parameters. Initially, the reaction was run at 180^{o}C for 20 minutes, providing little evidence of crystalline GeTe. The reaction time was then extended to 45 minutes keeping all other conditions the same. With no

favorable outcomes, the reaction temperature was then increased to 225^{o}C to achieve desirable results.

Synthesis of GeI_2 on Silicon <100> Substrate

GeI_2 was originally targeted as a precursor to GeTe. A composite slide consisting of a 100 nm Ge film on silicon <100> substrate was obtained. The slide was placed in a 20 mL septum cap vial and 0.15 grams of crystal I_2 were added. The vial was heated to 50^{o}C and a violet-pink gas sublimed from the iodine. The vial was allowed to sit for 24 hours before removal of the slide for XRD analysis.

The parameters of the reaction were then adjusted to move towards a solution-based route. 0.15 g I_2 were dissolved in 5 mL hexanes. A new slide was submerged in this solution for 24 hours under moderate mixing at 50^{o}C.

0.35 g I_2 were then dissolved in 5 mL octadecene to achieve a higher reaction temperature using a solvent with a higher boiling point. A new slide was submerged in this solution and heated for 24 hours under moderate mixing at 160^{o}C.

To remove possible oxide buildup that could hinder the reaction, the sonicative wash procedure described previously was performed on a slide. After pulling vacuum on a new vial and backfilling with argon, a degassed solution of 0.35 I_2 in 5 mL octadecene was added to the vial to submerge the slide. The reaction was heated to 160^{o}C for 24 hours under moderate mixing.

Preparation of TOP-Te Stock Solution

2.55 g Te was dissolved in 20 mL of trioctylphosphine and mixed under argon for several hours. The solution was subsequently heated to 120^{o}C and vacuum was pulled to

remove possible water vapor. The solution was backfilled with argon and heating continued to 220^{o}C or until Te fully dissolved.

Characterization.

All powder x-ray diffraction (XRD) analysis was completed using a Bruker D8 Advance X-Ray Diffractometer with a LynxEye 1-D-detector (CuKα radiation).

Results and Discussion

The first system tested was a 100 nm film of germanium deposited on a glass substrate. The attempt to convert the Ge film to GeTe resulted in the Ge film sliding off the glass substrate after exposure to the TOP-Te. The film broke up into smaller fine particles and then suspended in solution, which was subsequently decanted and centrifuged at 9,000 RPM for 5 minutes to collect a cake layer of the Ge particles. Any part of the germanium film that remained on the glass substrate was lightly scraped off for collection and added for analysis. An XRD analysis (Figure 3) showed no presence of germanium telluride. The right tail skewness of the pattern is due to the background noise signal of the glass substrate.

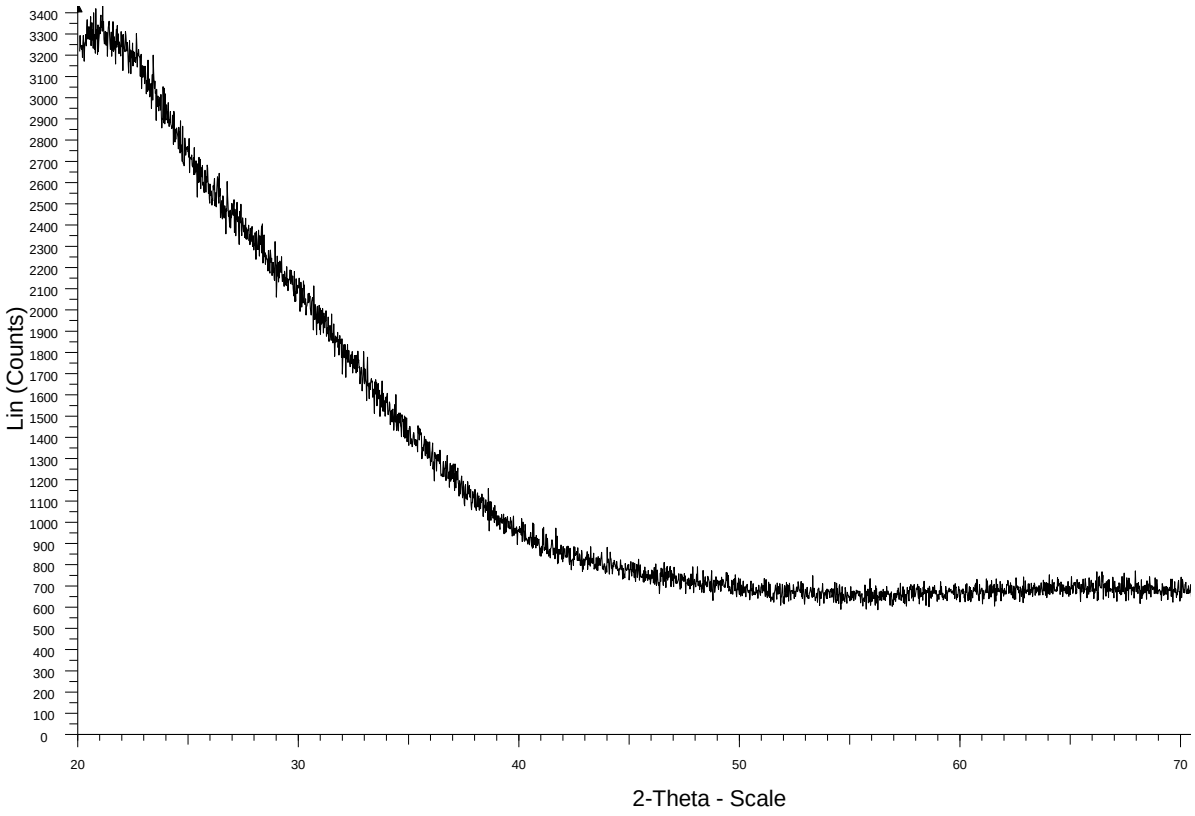

Figure 3. XRD pattern of 100 nm Ge film on glass substrate; no evidence of GeTe

A second, third, and fourth trial were run using a 100 nm, 200 nm and 200 nm Ge film on glass, respectively. In 3 of the 4 trials the germanium film dispersed into solution, and for all trials the XRD patterns produced were the same, marking the end of using the glass substrate due to its instability and unfavorable results.

The instability of the germanium film on the glass substrate may be explained by examining the interfacial bonding between the glass substrate and thin film. As the temperature of the reaction increased, the vibrational energy of the system overcame local Van der Waal forces and weak covalent bonds therefore releasing the film. TOP-Te may have also diffused through the thin film and reacted with the glass substrate to form

a stronger bond, effectively displacing the germanium layer. Although germanium can be deposited on glass, this does not necessarily confer stable adhesion.

Next, a germanium film on a silicon <100> substrate was used under the same conditions. The germanium film was much more stable on the new support and did not fall off into solution. This may be explained by the differences in lattice-mismatching of germanium and glass versus silicon, or possibly a weaker interaction between the TOP-Te and silicon support. After reaction completion, there was a distinct blue tint around a normally illustrious silver sheen. Figure 4 shows two trials repeated under the same conditions, compared against a baseline slide that had not been reacted.

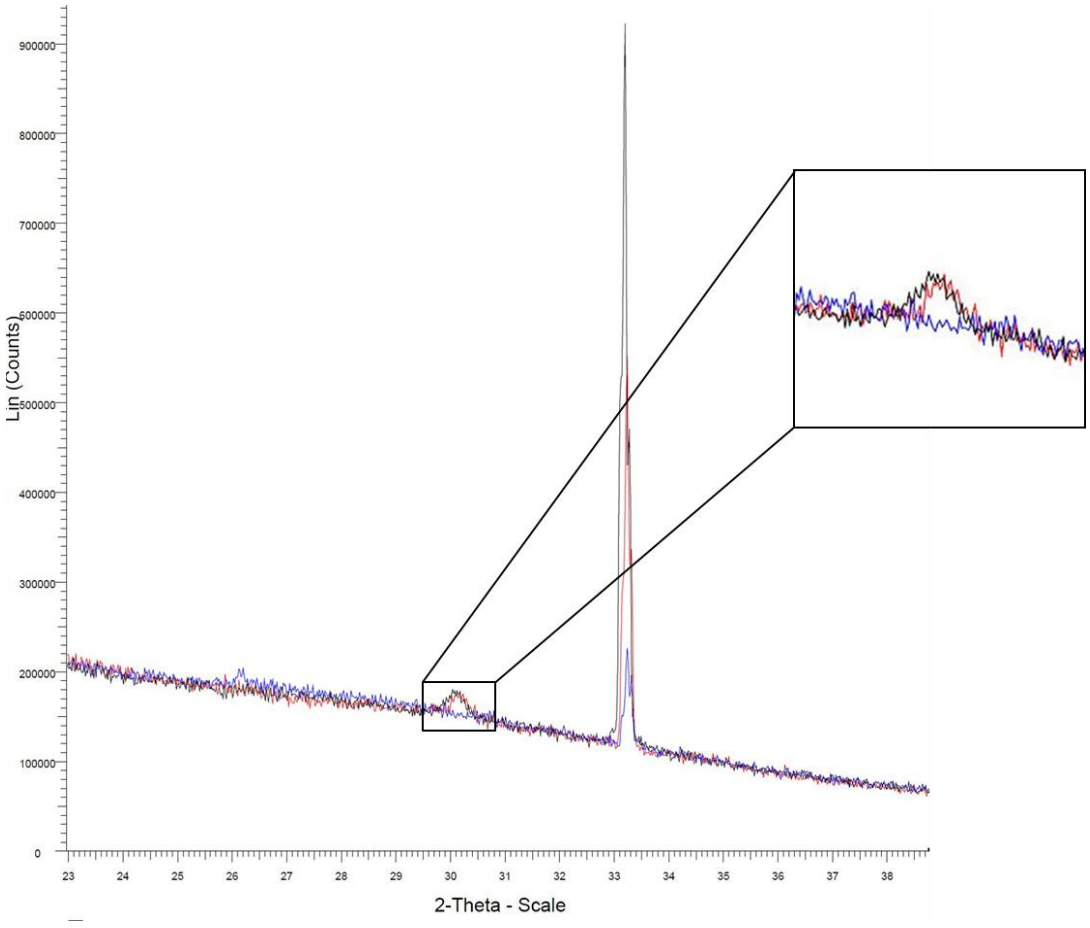

Figure 4. XRD patterns of 2 trials of Ge on Si <100> compared against unreacted baseline in blue

A sharp, high intensity peak is present slightly above 33^o 2-Theta due to the silicon substrate. However, at about 30^o 2-Theta there is a smaller peak that is not accounted for by the baseline. GeTe simulated peaks appear at approximately the same position, which may indicate the beginning of crystallization of GeTe. This can be further rationalized through the possibility of a preferred crystalline orientation with weak texture. It should be noted that in the analysis no other peaks with a relationship to GeTe were present.

A different approach was then taken to convert the germanium film to germanium telluride. Caldwell et al. reported the synthesis of GeTe using GeI_2 and TOP-Te[21], as well as others using similar techniques[22,12]. It was also demonstrated that germanium iodides could be prepared via sublimation of iodine at high temperature over germanium crystals[23]. If one could convert the germanium film to germanium iodide, it would serve as a valuable precursor to reaching the GeTe goal.

The first trial to convert the 100 nm germanium film on silicon <100> to GeI_2 was via a sublimation route under air. The iodine crystals sublimed and stayed in the gaseous phase for approximately 24 hours. Towards the end of the reaction, iodine crystals began to deposit at the top of the vial due to a temperature gradient. XRD analysis provided no evidence of crystalline GeI_2. In the second trial, the germanium slide was submerged in a solution of iodine in hexanes and allowed to mix under air for 24 hours at 50^oC. XRD analysis showed no presence of crystalline GeI_2. For run 3, the second trial was then repeated using the basic sonicative wash technique under argon and at 50^oC for 24 hours with no results. Runs 2 and 3 were then repeated using an octadecene solvent for a higher

reaction temperature. The reactions were heated to 160^{o}C for 24 hours under both air and argon, but ultimately neither yielded GeI_2.

The germanium film on silicon <100> substrate procedure was then restructured to run at a higher temperature and for a longer period of time. The solution was heated to 225^{o}C for 45 minutes before allowing to cool to room temperature. The slide became a very noticeable orange-blue and maintained its shine. XRD analysis produced the following results:

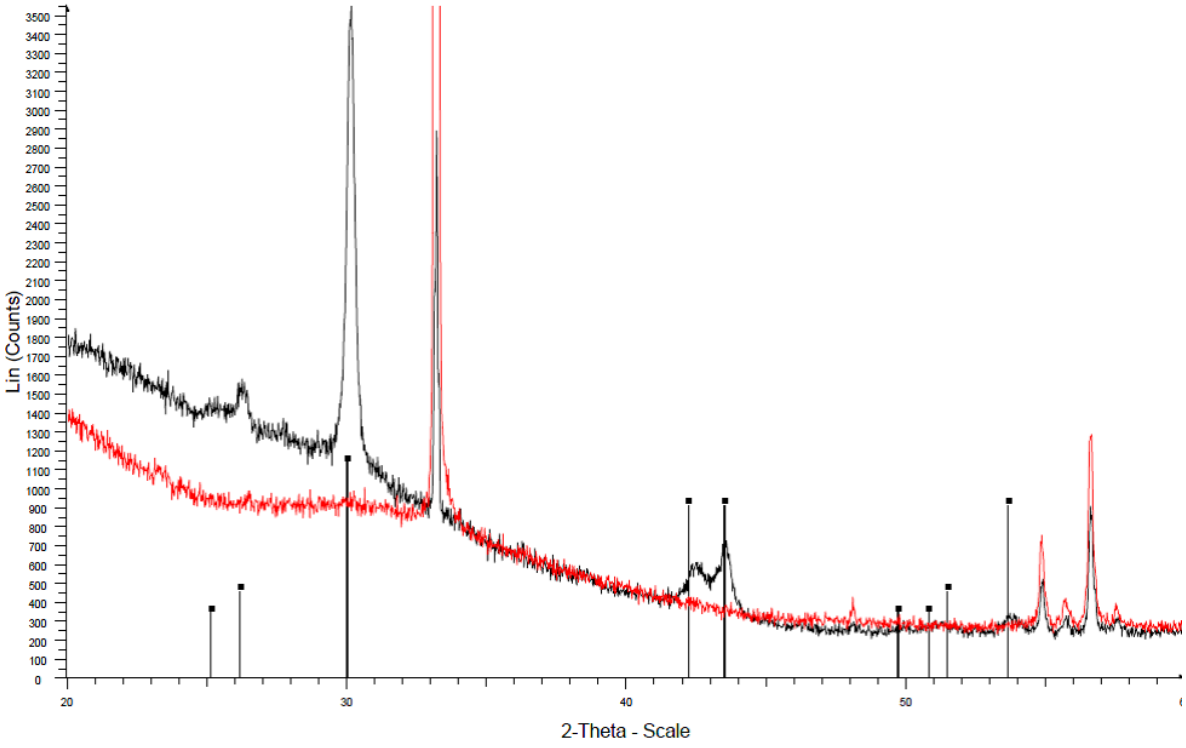

Figure 5. XRD pattern of GeTe on Si <100> in black. Database rhombohedral GeTe peaks provided. Baseline in red.

Comparison of the experimental slide, baseline, and simulated GeTe XRD patterns confirms the presence of crystalline GeTe. The intensities of the experimental slide pattern agree well with those predicted from the simulated XRD pattern.

An explanation for the success of this solution-route synthesis of GeTe may stem from the crystallization temperature of GeTe. Size has a profound effect on the amorphous-to-crystalline transition - bulk GeTe is known to crystallize at ~170 ^{o}C, whereas others have observed nanocrystal GeTe crystallization temperatures from 320 – 400 ^{o}C.[22, 23] It is possible that the reaction proceeds only at temperatures high enough to achieve GeTe crystallization, but one cannot rule out the possibility of amorphous GeTe residing on the substrate support.

Past samples were annealed under argon at temperatures ranging from 150 – 250 ^{o}C for 3 hours per trial to induce crystallization of amorphous GeTe films if present. However, the XRD analysis showed no change to the diffraction patterns indicating no crystalline GeTe. It has been observed that in many materials, the phase with the lowest surface energy becomes more favored than the thermodynamic stabilities in the bulk. Although amorphous versus crystalline surface energy data are not available for GeTe, Caldwell et al. reason the amorphous GeTe phase has a substantially lower surface energy than that of the crystalline phase[21,24]. Therefore, either no amorphous GeTe was present or one could not elicit the transition from amorphous GeTe to crystalline GeTe at the temperature/pressure conditions. No crystalline germanium peaks appeared because the crystallization temperature for poly-Ge films has been measured between 400^{o} – 500^{o}C for 20 hour annealing treatments[24].

Composite slides of germanium rods deposited on silicon <100> were then treated to the same conditions that provided GeTe. Figure 6 below shows the results:

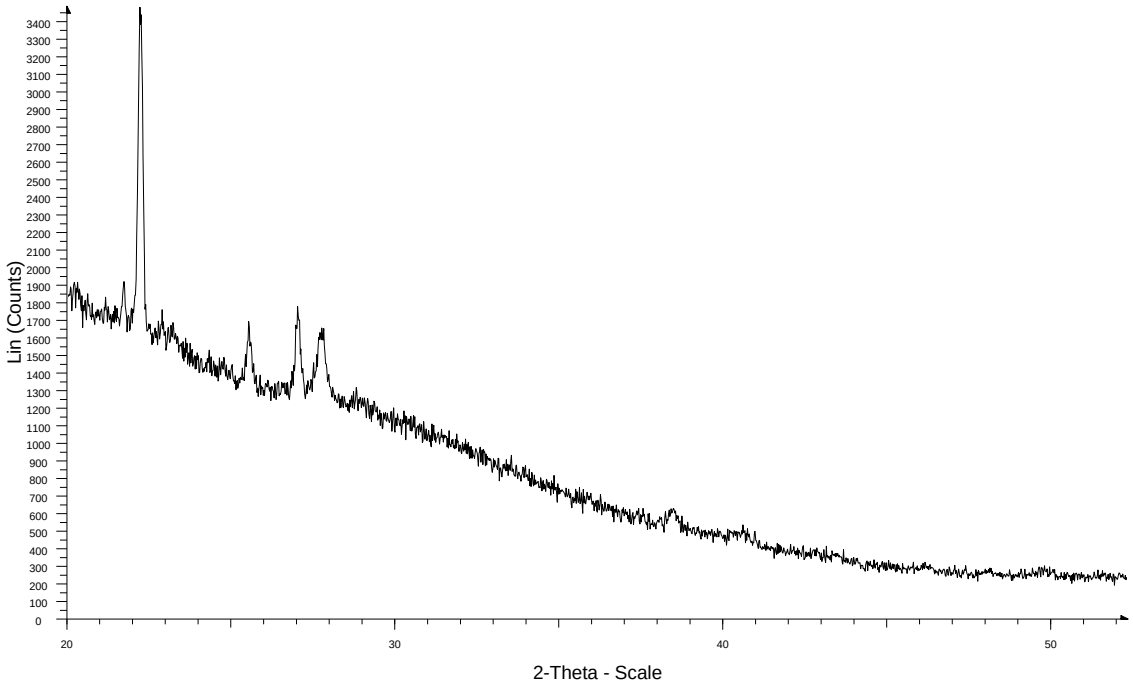

Figure 6. XRD pattern of Ge rods on silicon <100> support

The XRD pattern was the same before and after the reaction, indicating no crystalline GeTe. Peaks ranging from 20 to 30^{o} 2-Theta are due to the Ge rod structures. The slides were then annealed under argon at 250 ^{o}C for 3 hours but no crystalline GeTe was observed.

One of the inherent challenges of the experimental design was to avoid a surface layer of oxidized species on the germanium film. The oxygen-germanium bond is a barrier to entry – it takes up preferential bonding sites. Prabhakarn and Ohino have previously shown that thin wafers of germanium develop an oxide surface coating upon exposure to air at room temperature[25]. Air oxidation produces a mixture of oxides, with the tendency to form higher order oxides (GeO_2) due to environmental moisture effects.

A basic solution sonicative wash was applied to the composite slide to prevent previous buildup of GeO_x because the slides were stored in air, but the difficulty lied in

transferring the slide from the washing apparatus to the vial for reaction. A brief exposure period to air of approximately 10 seconds existed due to transferring the slide from the vial containing the basic solution to the new vial and pulling vacuum. In this time period, it is possible that oxidation of the surface layer of germanium atoms occurred, which could inhibit the conversion reaction. There could also be GeO_2 impurities within the sample itself, which presents a far greater challenge to overcome.

By no means is this investigative work exhaustive. One of the most significant difficulties, knowing whether amorphous GeTe was present, could be solved by using energy-dispersive X-ray spectroscopy (EDS) for chemical characterization and elemental distribution of the films. Extended X-ray absorption fine structure (EXAFS) studies show a difference in the Ge-Te bond length between amorphous and crystalline states, which can be used to determine percent crystallization of the film as well as GeTe presence.[26] X-ray photoemission spectroscopy (XPS) could also probe the electronic and chemical state of the product films. Because XPS is such a sensitive surface tool, it could detect oxide layers several nanometers deep.[27] It has been demonstrated that GeO_2 can be selectively removed from germanium surfaces through a warm water rinse due to its water solubility[25]; this capability opens the possibility to future oxide removal routes. Finally, atomic force microscopy (AFM) could probe the surface of the germanium film both before and after the reaction, examining for changes in physical properties such as surface texture that could give better insight into any changes occurring.

Conclusion

The work presented provides a framework for thin germanium films deposited on different substrate supports to react with TOP-Te and form germanium telluride, a prototype phase change material. The glass substrate was found to be an insufficient support for the germanium films due to stability and adhesion problems. Crystalline germanium telluride was synthesized on a silicon <100> support by reaction at high temperatures (225^{o}C) for an extended period of time (45 minutes). Germanium rods on a silicon <100> support, however, were not able to be converted to GeTe. The annealing of samples that possibly contained amorphous GeTe did not produce crystalline GeTe.

References

1) Yu, D.; Wu, J.; Gu, Q.; Park, H. *J. Am. Chem. Soc.* **2006,** *128*, 8148 – 8149.
2) Raoux, S.; Wełnic, W.; Ielmini, D. *Chem. Rev.* **2010,** *110,* 240–267.
3) Rabe, K. M.; Joannopoulos, J. D. *Phys. Rev. B* **1987**, *36,* 6631.
4) Akola, J.; Jones, R. O. *Phys. Rev. B* **2007,** *76,* 235201.
5) Bahl, S. K.; Chopra, K. L. *J. Vac. Sci. Technol.* **1969,** *6,* 561.
6) Luo, M.; Wuttig, M. *Adv. Mater.* **2004**, *16*, 439.
7) Detemple, R.; Wamwangi, D.; Wuttig, M.; Bihlmayer, G. *Appl. Phys. Lett.* **2003**, *83*, 2572.
8) Bahl, S. K.; Chopra, K. L. *J. Appl. Phys.* **1970**, *41*, 2196-2212.
9) Wuttig, M.; Yamada, N. *Nat. Mater.* **2007,** *6,* 824.
10) Solis, J.; Afonso, C. N. *Appl. Phys. A: Mater. Sci. Process.* **2003**, *76*, 331.
11) Lencer, D.; Salinga, M.; Grabowski, B.; Hickel, T.; Neugebauer, J.; Wuttig, M. Nat. Mater. **2008**, *7*, 972–977.
12) Buck, M. R.; Sines, I. T.; Schaak, R. E. *Chem. Mater.* **2010**, *22,* 3236 – 3240.
13) Alu, A.; Engheta, N. *J. Opt. A: Pure Appl. Opt.* **2008,** *10,* 093002.
14) Gholipour, B.; Zhang, J.; MacDonald, K. F.; Hewak, D. W.; Zheludev, N. I. *Adv. Mater.* **2013**, *25,* 3050 – 3054.
15) Leonhardt, U.; *Nat. Photonics* **2007,** *1,* 207 – 208.

16) Schurig, D.; Mock, J.J.; Justice, B. J.; Cummer, S. A.; Pendry, J. B.; Starr, A. F.; Smith, D. R. *Science* **2006**, *314,* 997 – 980.
17) Lezec, H. J.; Dionne, J. A.; Atwater, H. A. *Science* **2007,** *316,* 430 – 432.
18) Samson, Z. L.; MacDonald, K. F.; De Angelis, F.; Gholipour, B.; Knight, K.; Huang, C. C.; Di Fabrizio, E.; Hewak, D. W.; Zheludev, N. I. *Appl. Phys. Lett.* **2010,** *96,* 143105.
19) Zheludev, N. I.; Kivshar, Y. S. *Nat. Mater.* **2012,** *11,* 917-924.
20) Wolfsteller, A.; Geyer, N.; Nguyen-Duc, T.-K.; Das Kanungo, P.; Zakharov, N.D.; Reiche, M.; Erfurth, W. et al. *Thin Solid Films,* **2010,** *518,* 2555-2561.
21) Caldwell, M. A.; Raoux, S.; Wang, H.-S.; Wong, D.J.; Milliron, J. *J. Mater. Chem.* **2010,** *20,* 1285.
22) Arachchige, I. U.; Soriano, R.; Malliakas, C. D.; Ivanov, S. A.; Kanatzidis, M. G. *Adv. Funct. Mater.* **2011,** *21, 2737-2743.*
23) Zelenina, L. N.; Titov, V. A.; Chusova, T. P.; Stenin, Y. G.; Titov, A. A. *J. Chem. Thermodyn.* **2003,** *35,* 1601 – 1612.
24) Tsao, C.-Y.; Weber, J. W.; Campbell, P.; Widenborg, P. I.; Song, D.; Green, M. A. *Appl. Surf. Sci.* **2009,** *255,* 7028-7035.
25) Prabhakaran, K.; Ogino, T. *Surf. Sci.* **1995,** *325,* 263 – 271.
26) Andrikopoulous, K. S.; Yannopolous, S. N.; Voyiatzis, G. A.; Kolobov, A. V.; Ribes, M.; Tominaga, J. *J. Phys. Condens. Matter,* **2006,** *18,* 965 – 979.
27) Sun, X.; Yu, B.; Ng, G.; Meyyappan, M. *J. Phys. Chem. C,* **2007,** *111,* 2421 – 2425.

Chapter 2

Probing the Au-Fe_3O_4 Heterodimer System for Oxidation Catalysis

Introduction

In the mid-1980s, Masatake Haruta showed to the scientific community the remarkable catalytic activity of gold nanoparticles and laid the groundwork for future generations of research[1]. Once thought to be too chemically inert for catalytic applications, gold has become a subject of increasing interest because of the role it plays in various important catalytic processes such as the oxidation of CO at low temperatures, water gas shift and steam reforming, hydrogenation of unsaturated substrates, and more.[2,3] However, gold is not without its limitations; high cost and limited availability both contribute to the effort to make gold catalysts more efficient.[4]

One of the most common and straightforward methods to reduce used amounts of nanoparticle gold is porous support deposition. By loading onto high surface-area supports, one can use less catalyst while subsequently enhancing catalytic activity. It is believed that these enhanced catalytic effects stem from factors such as surface reconstruction around the junction interface and electron interaction/transfer across the interface.[5] However, problems arise with nanocatalysts on solid supports due to particle immobilization, which decreases the catalytically active surface area and reactivity of the catalytic species.[4] Catalyst recycling and reusability also becomes hampered by the time-consuming process of centrifuging/redispersion for catalyst separation from the reaction mixture. Another separate but significant problem is that support surface properties must

be compatible with the deposition conditions of the gold.[6] For example, to deposit Au nanoparticles from aqueous solution onto an oxide support, the pH of the impregnating solution must be adjusted to below the isoelectric point of the support surface[7]; otherwise, ionic adsorption onto the support will not occur[8].

An emerging solution to these support issues is magnetically separable heterogeneous catalysts. Au-Fe_3O_4 is a nanocatalyst in which the gold nanoparticle is directly linked to a similar sized iron-oxide domain. The iron-oxide substituent enhances catalytic activity while preserving the characteristics of an unsupported catalyst. The gold metal-oxide nanoparticles have exhibited catalysis in the areas of CO oxidation, H_2O_2 reduction, and nitroaromatic reduction, yet their magnetic property also eliminates the necessity of catalyst filtration. Additionally, these particles can be deposited on bulk support systems to further fine-tune an already active catalytic system. Au-Fe_3O_4 is a heterogeneous catalyst but has the benefits of a homogeneous one in that it can be dispersed throughout an entire solution without worry of traditional particle suspension or packed bed fluid dynamics.

Au-Fe_3O_4 has been synthesized with a variety of nanostructures including core/shell, flower-like, and dumbbell-like heterostructures (Figure 7). Core/shell Au-Fe_3O_4 particles have already made headway in areas such as biomolecule immobilization and detection[9] and MRI imaging,[10] while the flower-like structures have been used for an *in vivo* optical nanosensor for imaging protease expressions[11]. One of the more studied systems is the Au-Fe_3O_4 dumbbell nanoparticle, from herein also referred to as a dimer.

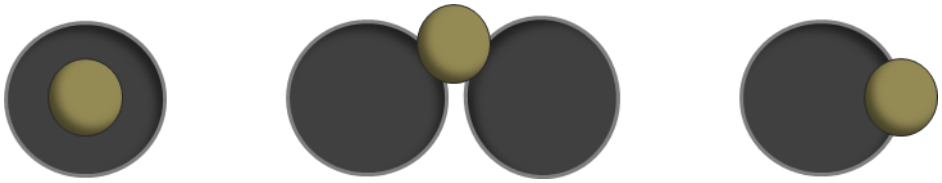

Figure 7. Possible Au-Fe_3O_4 nanostructures. Left to right - core/shell, flower-like, dumbbell-like

It has not yet been completely defined how the size dependence of the Au and metal-oxide affects the catalytic properties of the dimer as a whole. As nanoparticles get smaller, not only does their surface area increase but their electronic properties are also modified. When the de Broglie wavelength of the valence electrons approaches the same size as the particle itself, the quantum size effect takes place and the particles behave as zero-dimensional quantum dots[3]. Large variations of electrical and optical properties are observed that can be fine-tuned by adjusting the size of the particle. It has been reported that nanoparticle gold is catalytically active in the range from 2 to 50 nm^2, which raises the question of what size Au-Fe_3O_4 dimers are catalytically active and whether the size of the gold or the oxide domain takes precedent in catalytic activity. Lee et al. has demonstrated that increasing the gold domain size from 3 nm to 8 nm in Au-Fe_3O_4 dimers shows higher activity and stability after 100 cycles of H_2O_2 reduction, however the synergetic effects controlled not by the Au but by the Fe_3O_4 have not been well studied[12].

Another inquiry into the Au-Fe_3O_4 dimer system is how different supports influence chemical stability and catalytic activity. Gold nanoparticles physically dispersed on oxide supports are often unstable due to the lack of a metal-support interaction[13]. However, when the Au-Fe_3O_4 dimer is put onto an oxide support via a colloidal deposition method, it is believed that the already present gold/iron-oxide

binding interface coupled with the new support is strong enough to prevent deactivation from acid vapor and thermal sintering[13]. Furthermore, it has been shown that discrete-sized dumbbell Au-Fe_3O_4 nanoparticles display negligible catalytic activity in CO oxidation until the use of an oxide support,[14] and that the appropriate choice of support has significant consequences for CO conversion percentage[13]. These findings indicate a formation of new active sites by Au-Fe_3O_4-support interfaces and warrant a further investigation into the effect of the unique secondary interface between the heterodimer and the support.

Surface molecules such as adsorbing surfactants and binding ligands used during preparation of Au-Fe_3O_4 dimers are also of interest to examine because of the relative lack of literature available describing their effects on dimer synthesis and catalytic activity. Current preparation methods of Au-Fe_3O_4 dimers are grouped into the thermal decomposition technique using iron precursors such as iron pentacarbonyl, iron acetylacetonate, and the iron-oleate complex, all in the presence of Au seeds[4]. Also available is a procedure in which the gold nanoparticles are synthesized *in situ* via injection of $HAuCl_4$. The various reactions use different surfactants such as oleylamine, oleic acid, 1-octadecene, and 1,2-hexadecanediol, while the Au nanoparticle preparations use similar capping surfactants and stabilizing thiol-ligands. There is less attention given to describing how these surface molecules may affect the catalytic properties by interacting with active sites, so naturally it is of interest to examine them further.

In the following range of experiments, I probe the dumbbell-like Au-Fe_3O_4 heterodimer system and its ability to catalyze the aerobic oxidation of organic alcohols in common solvents. An oxidation approach was chosen because of the extensive previous

research done using Au nanoparticles as powerful catalysts for the oxidation of alcohols, aldehydes, amines, hydrocarbons, and more[15]. It is believed that an adjacent oxide constituent such as Fe_3O_4 gives rise to oxygen vacancies on the interfacial surface, thus becoming an active site for oxygen adsorption and activation[12]. Au-Fe_3O_4 dimers have also been shown to successfully oxidize CO both on and off a bulk support. I change numerous parameters such as Au and Au-Fe_3O_4 preparation methods, types of supports, substrates for oxidation, thermal ligand treatments, temperature, length, and media polarity of reaction conditions, and more to systematically determine the effects each has on possible catalytic activity.

Experimental

Materials.

The following chemicals were purchased and used without further purification. Hydrogen tetrachloroaurate (III) trihydrate (99.99%), triphenylphosphine (99%), biphenyl (99%), benzoic acid (99%), nitrosonium tetrafluoroborate (98%), trisodium citrate dihydrate (99%), and titanium (IV) oxide was purchased from Alfa Aesar. 1-octadecene (tech. 90%), oleylamine (tech. 70%), borane *tert*-butylamine complex (97%), 1-dodecanethiol (>98%), iron (III) acetylacetonate (>99.9%), oleic acid (>99%), benzyl alcohol (99.8%), *p*-xylene (99%), 1-2 hexadecanediol (90%), iron (0) pentacarbonyl (>99.99%), N, N-dimethylformamide (99.8%), 1-octanol (>99%), cinnamyl alcohol (98%), *trans*-cinnamaldehyde (99%), 4-methylbenzyl alcohol (98%), 4-

methylbenzaldehyde (97%), and cerium (IV) oxide were purchased from Sigma Aldrich. Chloroform (99.9%), ethyl ether (99%), dichloromethane (99.9%), ethyl acetate (99.5%), and sulfuric acid (95%) were purchased from EMD. XC-72 Vulcan carbon was obtained from E-TEK.

Methods.

Synthesis of Au Nanoparticles

Method 1. 100 mg $HAuCl_4$ were dissolved via sonication in 10 mL octadecene and 10 mL oleylamine. The solution was heated to 120^{o}C and mixed under air for 45 minutes. The gold nanoparticles were then isolated using EtOH addition and centrifugation at 8000 RPM for 8 minutes, and redispersed in 5 mL hexanes.

Method 2. 100 mg $HAuCl_4$ were added to a flask containing 10 mL chloroform and 2 mL oleylamine, and the solution was stirred for 10 minutes in air at 30^{o}C. A solution containing 80 mg TBAB and 100 μL of oleylamine dissolved in 2 mL chloroform was then subsequently added to the $HAuCl_4$-OAm mixture. The mixture was stirred at 30^{o}C for an additional hour. The gold nanoparticles were collected via addition of a 5:1 ethanol:methanol mixture and centrifuged at 8000 RPM for 8 minutes. The nanoparticles were then washed with EtOH and redispersed in 5 mL hexanes.

Method 3. All solvents were degassed with argon for 2 minutes prior to reaction introduction. 200 mg $HAuCl_4$ were added to a flask and vacuum was pulled with

subsequent argon backfilling. 7 mL of 95% EtOH were added under argon, followed by a precursor solution of 273 mg PPh_3 in 10 mL EtOH. The colorless reaction mixture was stirred for 2 minutes and the product was then filtered over a glass frit, washed 3 x 10 mL with Et_2O, and dried. The solid product was then dissolved in ~2 mL dichloromethane and recrystallized by slow addition of hexanes and cooling to -25^oC which yielded a white needled $AuCl(PPh_3)$ precipitate. 0.77 g of $AuCl(PPh_3)$ were then added to a solution of 75 µL dodecanethiol in 12.5 mL benzene. 130.45 mg TBAB were added to the solution, which was then mixed at 55^oC for one hour, and then allowed to cool to room temperature under air. Gold nanoparticles were collected by EtOH addition and centrifugation at 8000 RPM for 8 minutes. The gold nanoparticles were washed with EtOH and redispersed in 5 mL hexanes.

Synthesis of Au-Fe_3O_4 Heterodimers

Method A. A precursor solution of 70 mg $Fe(acac)_3$, 2.7 mL oleic acid, and 4 mL oleylamine was prepared in a 3-neck round bottom flask. Under a flow of argon, the solution was heated to 180^oC within 20 minutes, aged for 10 minutes, and then 5 mg of Au nanoparticles in 2 mL oleylamine were added. Shortly after, 1.33 mL of oleic acid were injected into solution. The solution was aged for 90 minutes at 180^oC under moderate mixing, and then subsequently heated to 300^oC within 25 minutes. The reaction mixture was then stirred for an additional 20 minutes and then allowed to cool to room temperature. The particles were centrifuged out with EtOH addition and centrifuged at 7000 RPM for 10 minutes, washed with EtOH, and dispersed in 5 mL hexanes.

To achieve the correct concentration of gold in oleylamine prior to injection into the solution, the original gold in hexane solution was rotovapped to dryness at 90 mbar and 50^{o}C. The mass of the remaining gold nanoparticles was then determined by taking the difference between the masses of the vial storing the nanoparticles and an empty, clean vial.

Method B. 1.90 mL oleic acid, 1.97 mL oleylamine, 2.58 g 1,2-hexadecanediol and 20 mL octadecene were added to a 3-neck round bottom flask. Under a blanket of argon, the mixture was heated to 120^{o}C and kept at that temperature for 20 minutes. 0.30 mL $Fe(CO)_5$ were subsequently injected into the solution. After 5 minutes, 40 mg $HAuCl_4$ in 0.5 mL degassed oleylamine and 5 mL degassed octadecene were injected. The solution was heated to reflux at 310^{o}C for 45 minutes. The solution was then cooled to room temperature and stirred in air for 1 hour. The nanoparticles were centrifuged at 7000 RPM for 10 minutes upon isopropanol addition, redispersed in hexanes, centrifuged again at 7000 RPM for 10 minutes upon EtOH addition, and then redispersed in 5 mL hexanes with 0.05 mL oleylamine for added stability.

Catalytic Experiments.

50 µL Au-Fe_3O_4, 50 µL benzyl alcohol, and 2 mL of p-xylene were added to a 20 mL septum cap vial. The vial was purged with O_2 for 10 minutes, and then kept under a blanket of O_2. The solution was heated to 100^{o}C and vigorously mixed for 1 hour. After cooling to room temperature, 250 µL of a 1.92 M biphenyl standard were added. The solution was then filtered over a silica column to remove remaining catalyst, washed with

ethyl acetate, and collected for GC analysis. All Au-Fe_3O_4 particles were disposed of after catalytic reactions – none were recycled.

Catalysis reactions were also run under the same conditions but for a longer period of time (24 hours) and at higher temperatures (180^{o}C and 204^{o}C). 1-octanol, cinnamyl alcohol, cinnamaldehyde, 4-methylbenzyl alcohol, and 4-methylbenzaldehyde were also used as substrates under the original conditions.

Phase Transfer of Au-Fe_3O_4 Heterodimers to Polar Media

Using $NOBF_4$. 500 µL of Au-Fe_3O_4 heterodimers were added to a 20 mL vial. Hexanes was added to dilute the sample to 1 mL total volume. 1 mL of DMF was added to the solution, followed by addition of 13 mg $NOBF_4$. The reaction was stirred vigorously for 10 minutes and then allowed to settle. 20 mL of toluene was added to the biphasic system to precipitate the nanoparticles. The resulting suspension was centrifuged at 7000 RPM for 3 minutes, the supernatant was decanted, and the particles were resuspended in DMF. The particles were then purified by a 22 mL 1:1 mixture of hexanes:toluene, centrifuged at 7000 RPM for 3 minutes, and redispersed in 400 µL DMF.

Using Sodium Citrate. 1.3 mL of Au-Fe_3O_4 heterodimers in hexanes (~5 mg/mL) were rotovapped to dryness at 100 mbar and 45 ^{o}C for 30 minutes. The particles were then washed 3 x 3 mL with a 1:2 mixture of hexanes:ethanol. The remaining suspension was again rotovapped to dryness and dispersed in a minimal amount of hexanes. A copious amount of ethanol was added to crash out the dimers, which were subsequently centrifuged out at 8000 RPM for 5 minutes. The suspension was put under vacuum for 30

minutes to remove any residual ethanol. 0.971 g of sodium citrate were then added to a minimal amount of deionized water. This mixture was reacted with the dimers for approximately 10 minutes under heavy sonication. The particles were then redispersed in 1 mL of deionized water.

Loading Au-Fe_3O_4 onto a Support

400 µL of Au-Fe_3O_4 heterodimers were added to a 20 mL vial and stirred at 1200 RPM. 19.5 mg of Vulcan carbon were slowly added. The reaction was stirred for 1 hour. The mixture was rotovapped to dryness, suspended in 4 mL EtOH, and micro-centrifuged at 7000 RPM for 3 minutes. The sample was then decanted, resuspended in EtOH, and centrifuged again. After decanting, the sample was washed with EtOH, which was then removed via rotovap. The solid sample was vacuumed for 1 hour to remove any residual EtOH. The black powder was then weighed in an alumina crucible and heated under N_2 in the TGA/DSC (ramp rate – 10 ^oC/min, temp – 450 ^oC, hold time – 1 hour). Other trials were also calcined under air rather than N_2 using the same parameters at 350, 450 and 550 ^oC.

In addition, titanium (IV) oxide and cerium (IV) oxide were also used as supports in the same proportions as Vulcan carbon.

H_2SO_4 Treatment

15 mg of Au-Fe_3O_4 loaded onto Vulcan carbon and 4 mL of 0.25 M H_2SO_4 were added to a 20 mL vial. The solution was sonicated under air for 30 minutes. An ample

amount of deionized water was then used to wash any remaining H_2SO_4 from the particles. The final product was collected via centrifugation.

Characterization.

Transmission electron microscopy (TEM) images were obtained from a JOEL 1200 EX II operating at 80 kV. All powder x-ray diffraction (XRD) analysis was completed using a Bruker D8 Advance X-Ray Diffractometer with a LynxEye 1-D-detector (CuKα radiation). Gas chromatography was performed on an Agilent 5890 Series II GC with a Supelco SB 5 column and FID detector.

Results and Discussion

The initial step to synthesizing the Au-Fe_3O_4 heterodimers was to prepare the precursor gold nanoparticle seeds. Three separate procedures were used, each applying different reagents for nanoparticle synthesis. Method 1 used oleylamine and octadecene surfactants but produced agglomerated nanoparticles that displayed neither homogeneity nor monodispersion, which can be seen in Figure 8.

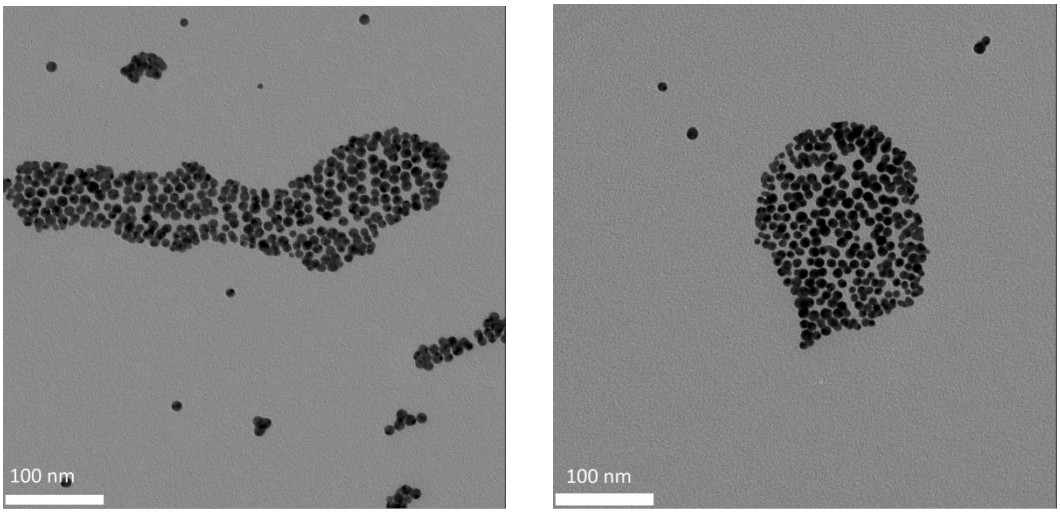

Figure 8. TEM images of OAm/ODE-capped Au nanoparticles with diameter size of 5.1 – 11.8 nm

Method 1 seed diameters ranged from 5.1 – 11.8 nm with sample mean $\mu = 9.3$ nm and standard deviation $\sigma = 1.6$ nm ($n = 40$). The poor particle boundary definition coupled with the clustering effect suggests the relatively weak surfactants were unable to stabilize the gold nanoparticles during synthesis. A second method was employed using only oleylamine as a surfactant in hopes to produce a more definitive product. These results can be seen in Figure 9 below.

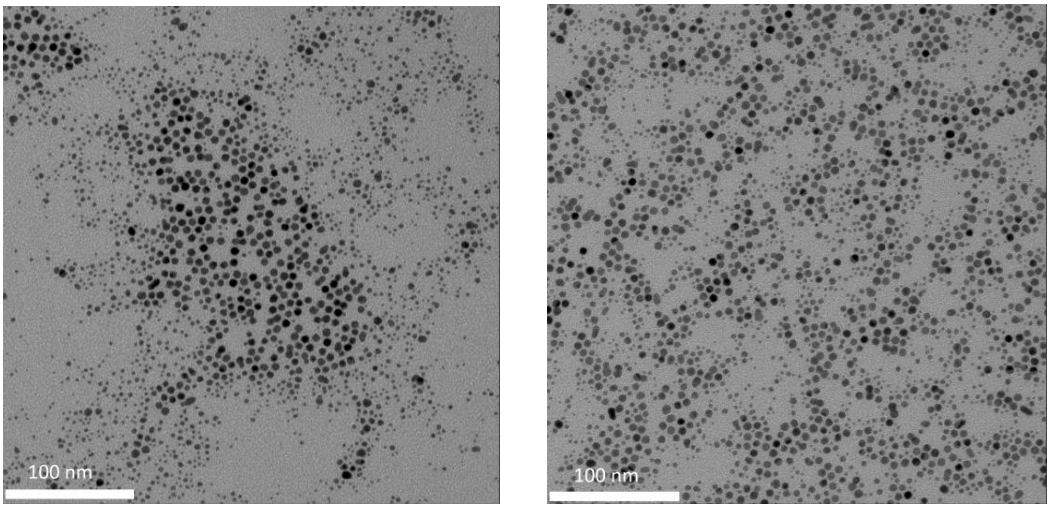

Figure 9. TEM images of OAm-capped Au nanoparticles with diameter size of 2.1 – 7.0 nm

Method 2 seed diameter ranged from 2.1 – 7.0 nm with a sample mean $\mu = 4.3$ nm and standard deviation $\sigma = 1.5$ nm ($n = 40$). While these particles are not agglomerated such as those in Figure 8, they are not uniformly distributed and the variance among diameter size leaves higher size control to be desired. A third method using dodecanethiol as a surfactant was also tested for gold nanoparticle synthesis. The nanoparticles produced ranged from 6.1 – 7.4 nm in diameter and were much more well shaped ($\mu = 6.8$ nm, $\sigma = 0.4$ nm, $n = 40$). The strongly binding thiol capping reagent provided a system for both morphology and size control. TEM imaging analysis (Figure 10) shows discrete particles.

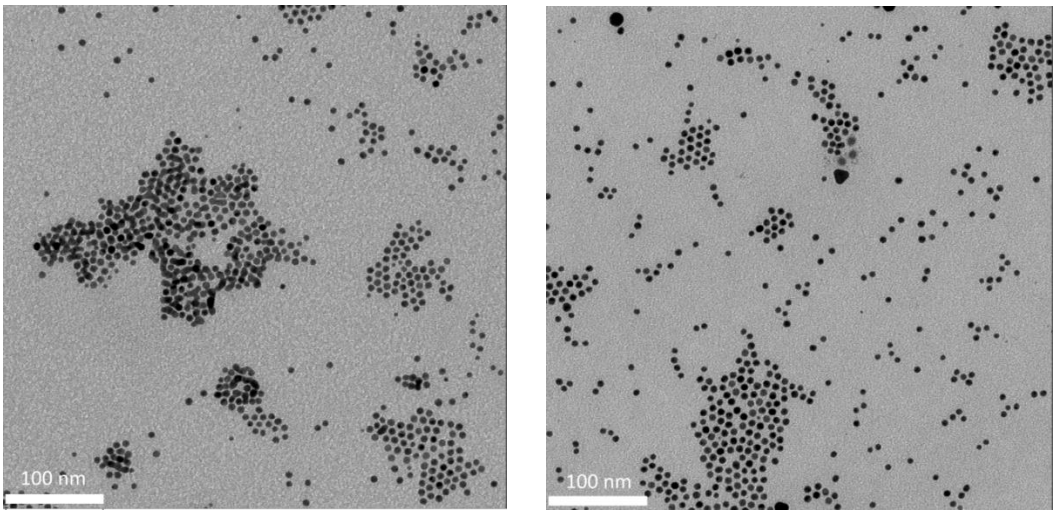

Figure 10. TEM images of dodecanethiol-capped Au nanoparticles with diameter size 6.1 – 7.4 nm

XRD analysis was performed on Method 3 nanoparticles to confirm the presence of gold. Comparison between the experimental pattern and a simulated Au XRD pattern shows a strong agreement between the two intensities, indicating the presence of gold (Figure 11).

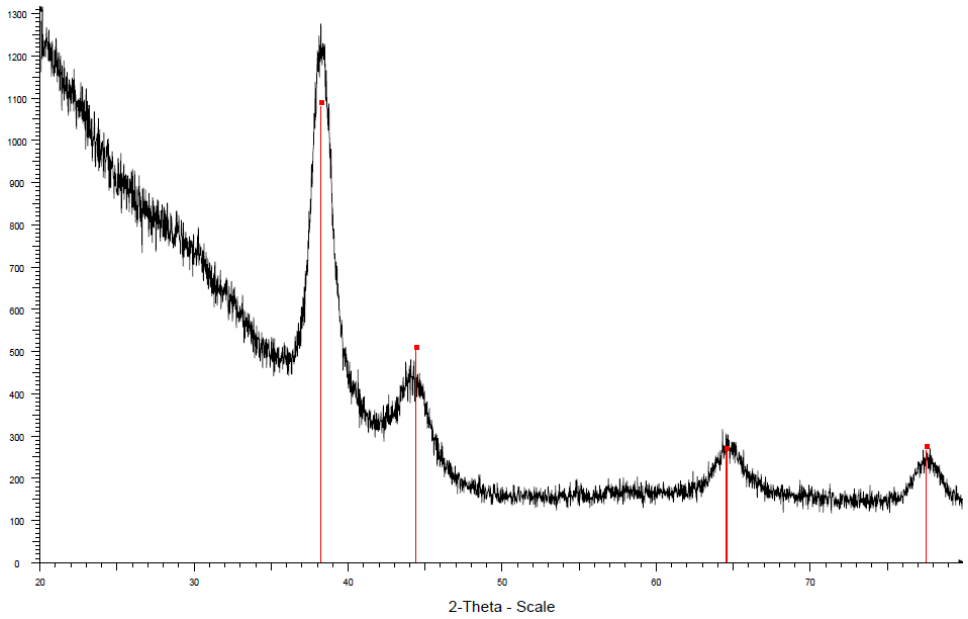

Figure 11. XRD pattern of dodecanethiol-capped Au NP in black. Database Au peaks provided in red.

With suitable Au precursor seeds available, Au-Fe_3O_4 heterodimers were then synthesized using a published procedure (Method A). One of the inherent challenges in the synthesis was process control of the heating apparatus. Both a steady ramping rate and temperature stabilization proved difficult to maintain; it took approximately 15 minutes longer to reach both 180^{o}C and 300^{o}C without overshooting the desired set point. Appreciable error was also introduced into the procedure when injecting 5 mg of Au in 2 mL oleylamine into the solution because of the limited sensitivity of the digital scale available.

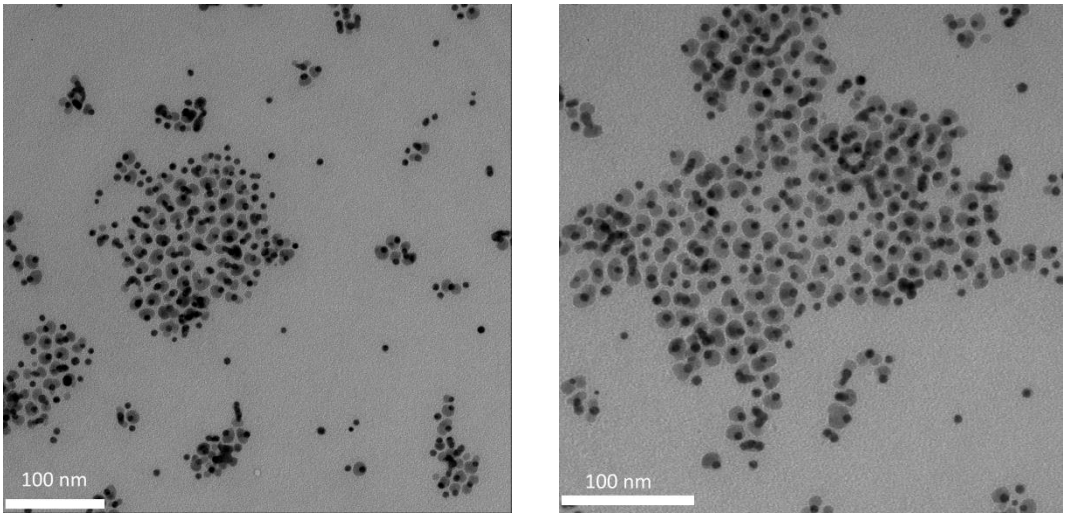

Figure 12. TEM images of Au-Fe_3O_4 heterodimers, Method A

Figure 12 shows a mixture of both dimer and flower-like Au-Fe_3O_4 structures. Although the extra metal-oxide domains may initially indicate too high a ratio of the iron precursor to gold seeds, the free gold nanoparticles elsewhere suggest the thermal decomposition was not completely uniform across the system and seeded growth was only partially achieved. Although not morphologically ideal, the Au-Fe_3O_4 heterostructures were tested for catalytic activity nonetheless.

The catalytic reaction was run for 1 hour at 100^{o}C using a benzyl alcohol substrate and the solution was filtered through a silica column with an ethyl acetate wash to remove any nanoparticles. Although the Au-Fe_3O_4 heterostructures were (weakly) magnetically separable, this filtering was used to ensure no contamination of the gas chromatography column during product analysis. Gas chromatography was chosen as an ideal analytical technique due to its quick and efficient qualitative analysis of benzaldehyde and benzoic acid presence. Prior to catalyst reaction, individual GC assays were run on each component of the reaction mixture to quantitatively determine elution

time; presence of an unknown peak after the catalyst reaction would indicate a reaction occurred. The results of the catalytic reaction are shown in the gas chromatogram below, with corresponding peaks assigned.

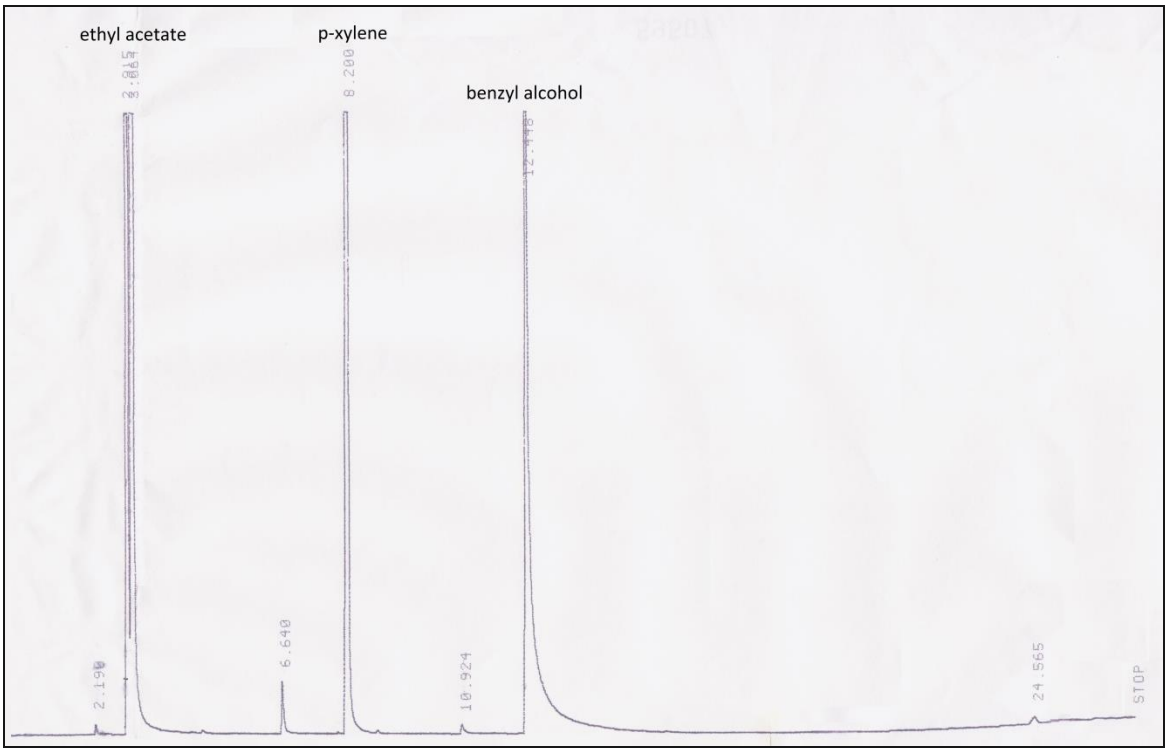

Figure 13. Gas chromatograph of Au-Fe_3O_4 dimer (Method A) test for catalytic oxidation of benzyl alcohol

It can be seen that the larger, more polar constituents elute slower through the column as expected. However, neither benzaldehyde nor benzoic acid was present indicating no oxidation took place. The very small peaks around 6.6, 10.9 and 24.6 minutes are due to small impurities in the reagents.

A benzoic acid in *p*-xylene solution was then run through the silica column to determine whether or not the benzoic acid adhered too strongly to this column, which would render it immobile and possibly explain the lack of benzoic acid in Figure 7.

However, NMR analysis showed that the benzoic acid solution passed completely through the silica column.

The gold seeds were then used in two additional attempts to synthesize the Au-Fe_3O_4 heterodimers under the same procedure (Method A), but neither trial produced well defined particles. Regardless, both sets of particles were tested for catalysis but neither showed signs of oxidation.

A novel, one-pot synthesis approach was then taken from a published procedure (Method B) to synthesize the Au-Fe_3O_4 heterodimers[10]. This technique benefitted from the fact the gold nanoparticle domain was synthesized *in situ* by $HAuCl_4$ injection, so precursor gold seeds did not have to be pre-made. Figure 14 displays the TEM analysis.

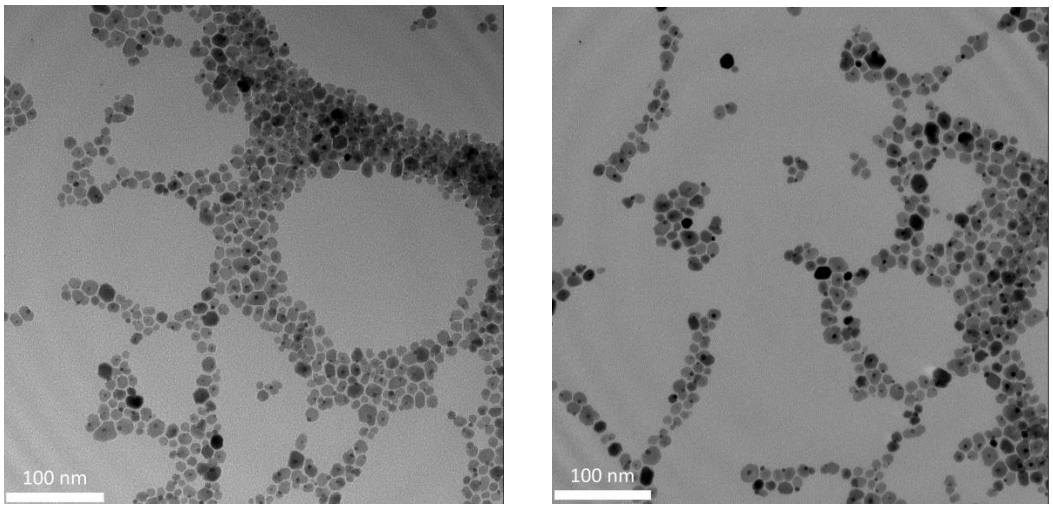

Figure 14. TEM images of Au-Fe_3O_4 nanostructures, Method B

The synthesized particles showed a mixed array of dimers, trimers, core/shell and other irregular structures. The lack of morphological control can be explained by the delicacy of the preparation method. Using the same Au-Fe_3O_4 procedure, George et al. found that varying the reaction temperature and reaction time by small intervals of 20^oC and from 30 minutes to 4 hours initially produced core/shell nanoparticles that evolved

into asymmetric metal/metal-oxide core/shell morphologies and heterodimers.[16] These findings support the position that the system's sensitive nature fails to provide a reliable and easily reproducible procedure of one-pot synthesis.

The Au-Fe_3O_4 nanoparticles synthesized via Method B were tested as a catalyst for benzyl alcohol oxidation, but again no oxidized species were found. It is important to note that a biphenyl standard was used for GC analysis from this point forward for a more quantitative method of determining possible selectivity and yield. The gas chromatogram with appropriate labeling is found in Figure 15.

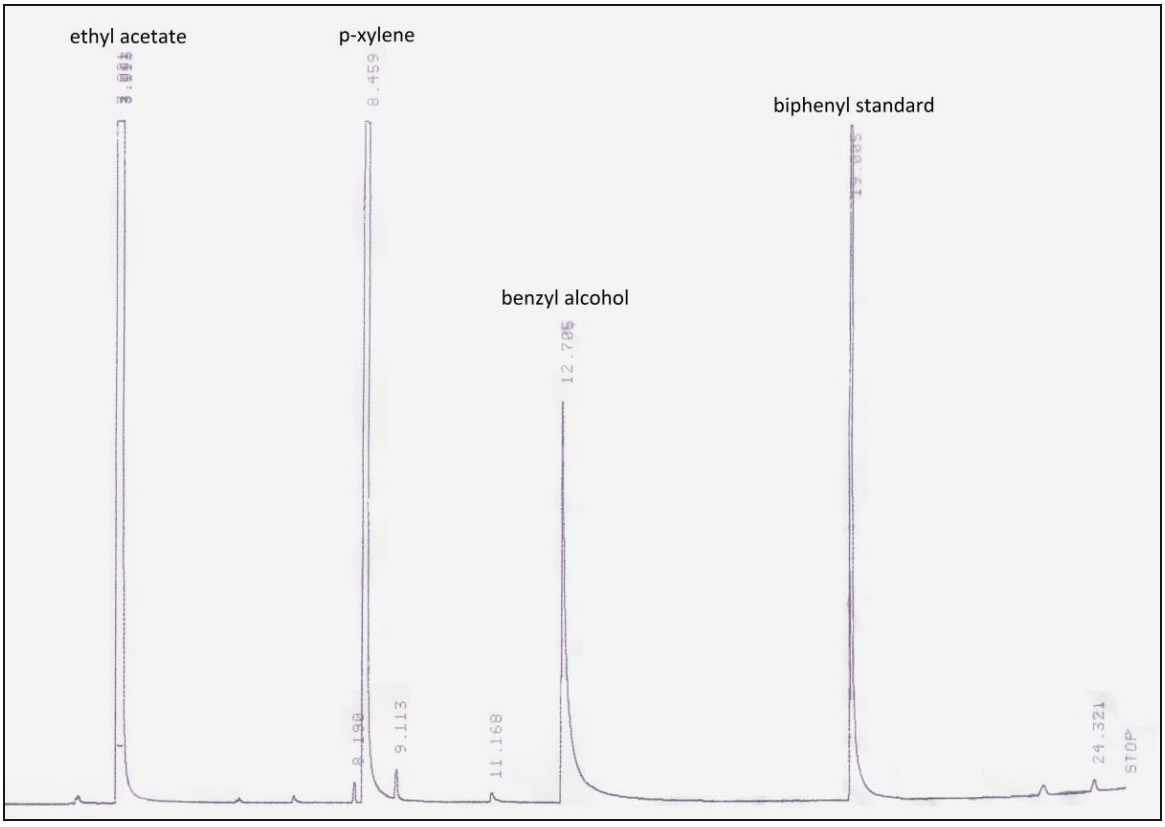

Figure 15. Gas chromatograph of Au-Fe_3O_4 dimer (Method B) test for catalytic oxidation of benzyl alcohol

Focus was then placed on finding a reproducible procedure for Au-Fe_3O_4 heterodimer synthesis with consistent morphology control. Method A was adapted to use

a Schlenk flask rather than a 3-neck round bottom flask. Separate reactions were run using the same conditions – however one reaction utilized a reflux condenser connected to a gas bubbler which created a flow of argon, while the other setup used only a septum cap which provided a blanket of argon. Both reactions proceeded normally, but a semi-transparent white gas evolved in the solution's headspace in the non-reflux setup at approximately 250^{o}C en route to 300^{o}C. This gas, which was most likely acetylacetonate decomposition products and/or oleylamine impurities boiling out of solution, gently diffused away upon reaching the temperature set point and was not observed in the reflux setup.

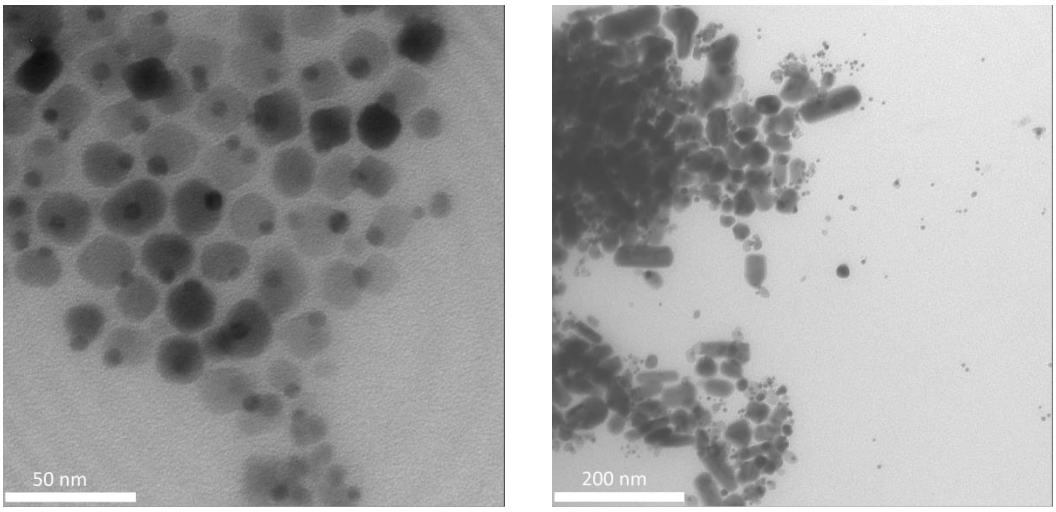

Figure 16. TEM images of non-reflux (left) and reflux (right) Au-Fe_3O_4 nanoparticles, adapted from Method A

It can be seen in Figure 16 the non-reflux setup produced dimers with consistent gold and iron-oxide domain sizes, whereas the reflux setup resulted in an agglomerated mix of particles that do not resemble the Au-Fe_3O_4 template nor have a defined boundary.

Although interest was placed in the non-reflux experimental dimers, both products were tested for oxidation catalysis with neither ultimately showing any activity.

With suitable Au-Fe_3O_4 dimers available, the catalysis reaction was restructured to run at higher temperatures and for longer periods of time. Initially, two catalysis reactions were set up so that each ran for 24 hours but one did not contain the Au-Fe_3O_4 nanoparticles as to provide a control comparison. Neither of these lengthened tests showed GC results that differed from previous trials. The catalysis reaction was then run at 180^{o}C for 1 hour to invoke catalysis, but this too did not prove fruitful. The setup was then modified to include a reflux condenser and the catalysis reaction was run at 205^{o}C, the boiling point of benzyl alcohol, but this also did not provide favorable results.

Because probing the catalytic system via both time and temperature did not influence results, the catalytic reaction was then altered to use a polar media. The majority of procedures to synthesize tunable nanoparticles often employ long hydrocarbon chain molecules such as oleic acid or oleylamine to stabilize the particles and prevent aggregation in a nonpolar, hydrophobic solvent. These bulky organic ligands also create an insulating barrier between the particles and outside molecular species as to block active catalytic sites. A solution to this problem is to apply a surface treatment to the original organic ligand moieties and exchange them with an inorganic anion to enable full dispersion in polar solvents. A published procedure was used to transfer the heterodimers to a dimethylformamide solvent while retaining all shape and size control[17]. The motive behind this was to remove any long-chain surfactants as well as possible thiol ligands from the original Au seed preparation that may have saturated the Au-Fe_3O_4 surface; in doing so, there would be increased surface area exposure promoting enhanced catalytic activity.

After transferring the dimers from hexanes into DMF, the catalysis reaction was run under the same standard conditions but used DMF rather than *p*-xylene as the solvent. GC analysis indicated no signs of benzaldehyde or benzoic acid. Two possible scenarios may explain the inactivity – the polar capping reagent over-saturated the dimer surface like the organic ligands, or the $NOBF_4$ was not strong enough to replace the previous surfactants. To address the first issue, the amounts of $NOBF_4$ and DMF were systematically reduced until a phase change no longer occurred. In each of these trials, the dimers in the polar solvent did not display catalytic activity, likely indicating that oversaturation was not the problem.

A second phase-change reaction procedure was then employed that used a sodium citrate reagent rather than $NOBF_4$. The sodium citrate method provided a facile preparation for water-soluble, magnetic nanoparticles. The dimers were transferred into H_2O and a standard catalytic test using H_2O as the solvent was run. No oxidized species were present in the gas chromatograph.

Because changing the solvent polarity did not elicit favorable results, the catalysis reaction was next run under neat conditions (no solvent) so that benzyl alcohol was the only medium for reaction. These conditions helped to eliminate the possibility of the *p*-xylene solvent blocking the dimer surface and insulating it from access to the benzyl alcohol substrate. However after workup and GC analysis, results showed no presence of oxidation.

The Au-Fe_3O_4 dimers were then tested for catalytic oxidation of separate substrates including 1-octanol, cinnamyl alcohol, cinnamaldehyde, 4-methylbenzyl alcohol, and 4-methylbenzaldehyde. These compounds were chosen based on availability,

pricing, and most importantly their differing molecular structuring. These substrates had advantageously high relative boiling points so that the catalytic reactions could be pushed at aggressively higher temperatures. Aldehydes were also chosen because of their already oxidized substituents, which may provide an easier oxidation route to a carboxylic acid product. Each new substrate was screened using GC analysis to confirm there was no overlap between previous elution times of the biphenyl standard, ethyl acetate, and *p*-xylene solvent. The same catalytic reaction procedure was run for each substrate using dimers from the same stock solution, but none showed signs of oxidized products.

After recognizing that altering the reaction conditions, solvents, and substrates was not proving successful, the system was pushed toward dimer support deposition in an effort to induce oxidation catalysis. The heterodimers were initially deposited on a Vulcan carbon support and the dried powder was then placed in a tube furnace for rapid thermal treatment at 450 ^{o}C. Wu et al. have shown that dumbbell Au-Fe_3O_4 nanoparticles deposited on TiO_2 were catalytically inactive for CO oxidation prior to thermal treatment, and suggest that organic residue is deleterious to the effective contact between the dimers and any support[14]. The thermal treatment was used to remove remaining oleylamine or oleic acid surfactant still present on the Au-Fe_3O_4 surface.

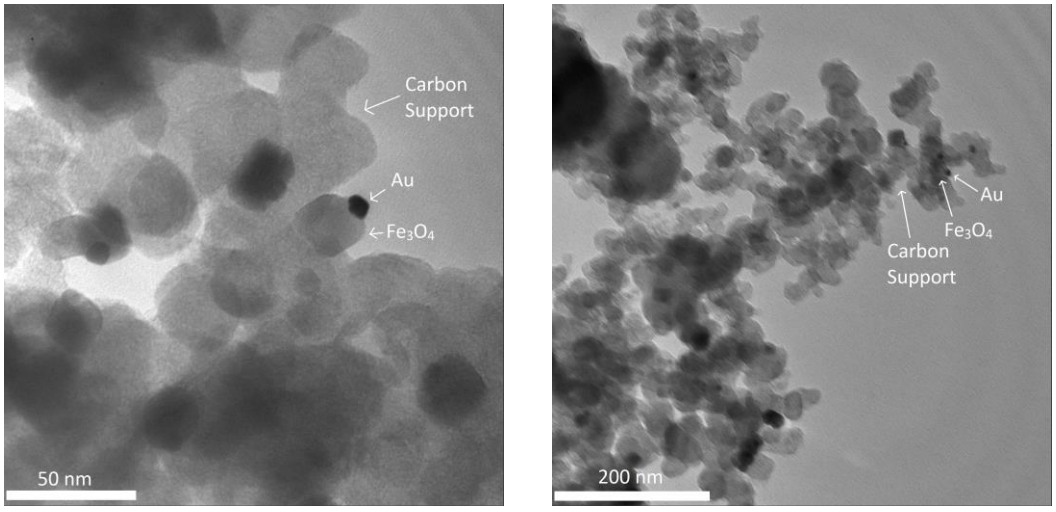

Figure 17. TEM images of Au-Fe_3O_4 loaded onto Vulcan carbon support

It can be seen that there is a relatively small amount of Au-Fe_3O_4 nanoparticles compared to the carbon support. The particles deposited on carbon were tested for catalytic activity but a GC assay showed no indication of any. The Au-Fe_3O_4 dimers were then deposited on carbon again and thermally treated at a higher temperature of 550 ^oC for the same period of time. The heat treatment protocol was selected based on published literature that shows evidence of increased Au-Fe_3O_4 catalytic activity when thermally treated at these temperatures[14]. The particles did not catalyze oxidation of any of the substrates.

There were two major concerns regarding the support loading and thermal treatment. The first problem was no available instrument could detect the exact interactions between the Au-Fe_3O_4 nanoparticles and the support. Figure 18 gives three possible interactions, and it is not known whether position (1), (2), or (3) is favored during support deposition and which one, if any, favors oxidation catalysis. Secondly, the thermal treatment may cause a high degree of dimer-support interface breakage at higher

temperatures. It can reasonably be expected that at a certain temperature there is more harm done by breaking interface bonds than good by removing remaining barrier ligands. In case the thermal treatment was inducing interface bond breakage, a set of dimers deposited on carbon was not heat-treated but these particles also did not exhibit oxidation catalysis.

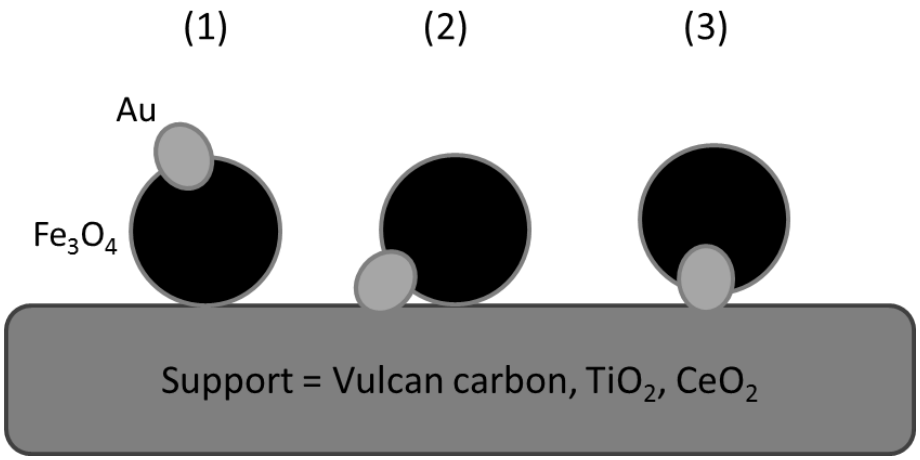

Figure 18. Three possible dumbbell-support interactions; adapted from Reference 3

The thermal treatment was then reconfigured to run under air rather than nitrogen in a calcination effort to remove possible organic species. The composite particles on carbon were calcined at 350, 450, and 550 ^{o}C for the same amount of time as previously, but none of these sets of particles showed catalytic activity. However, Figure 19 demonstrates that the support deposition protects against thermal sintering in both the air and nitrogen treatment.

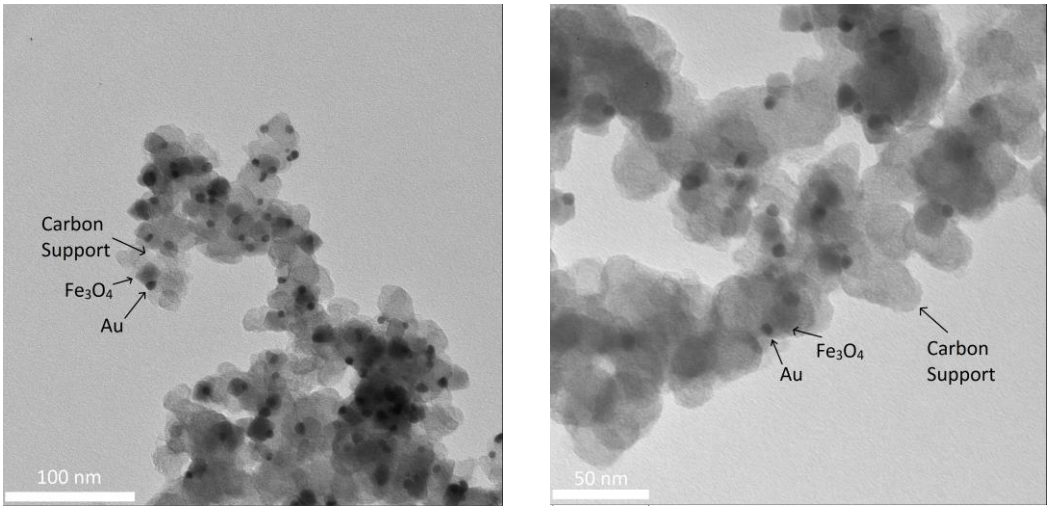

Figure 19. TEM images of Au-Fe_3O_4 loaded onto carbon thermally treated under air (left) and N_2 (right)

Because ligand blocking was still a concern, Au-Fe_3O_4 dimers were deposited on the Vulcan carbon and treated with $NOBF_4$, followed by calcination at increasing temperatures. This system provided a two-pronged approach for surfactant removal, but ultimately did not prove successful for substrate oxidation.

Using a similar procedure, the Au-Fe_3O_4 particles were next deposited on both TiO_2 and CeO_2. These two supports were chosen because literature precedent showed gold catalysis activation on them, and they could easily be substituted into the colloidal deposition method for convenient applicability.

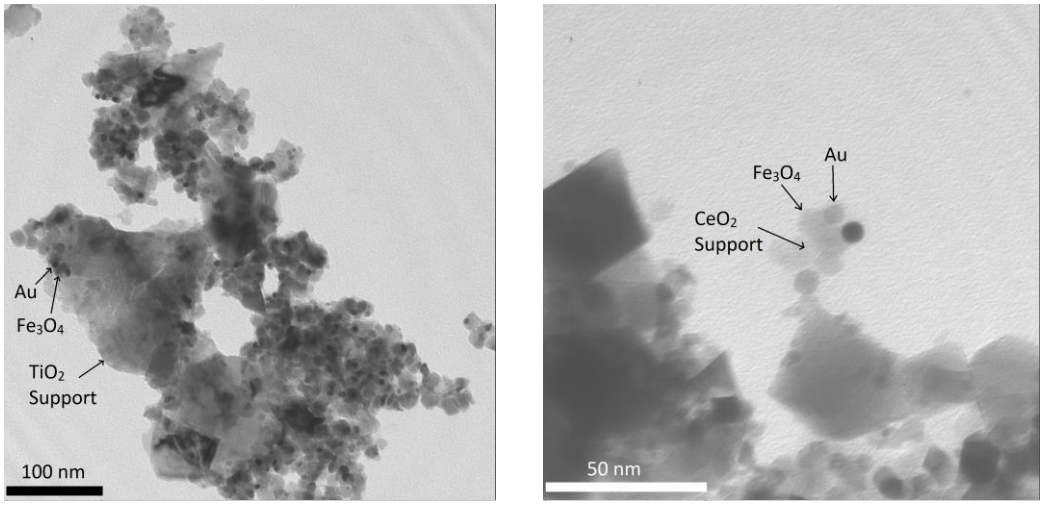

Figure 20. TEM images of Au-Fe_3O_4 particles loaded onto TiO_2 (left) and CeO_2 (right)

The nanoparticles were more stable and abundant on the TiO_2 support. TEM analysis showed particles loosely bound to the fringes of the CeO_2 support, suggesting weak interface contact. Both support systems were thermally treated in the same manner as the carbon support, but both systems did not show signs of substrate oxidation.

One of the possible problems associated with the growth of the iron-oxide domain off the gold seed is that the oxide may not completely separate from the gold, leaving behind a thin (< 5nm) iron-oxide shell. This hypothetical shell could block access to the gold surface, causing a detrimental effect to catalysis. To test this possibility, the dimers deposited on carbon were given a brief sulfuric acid wash which would etch away the iron-oxide shell, if present[12]. It was important to use supported heterodimers so that gold aggregation would not occur. TEM imaging of the particles before treatment are available in Figure 19, while post-treatment pictures are found below.

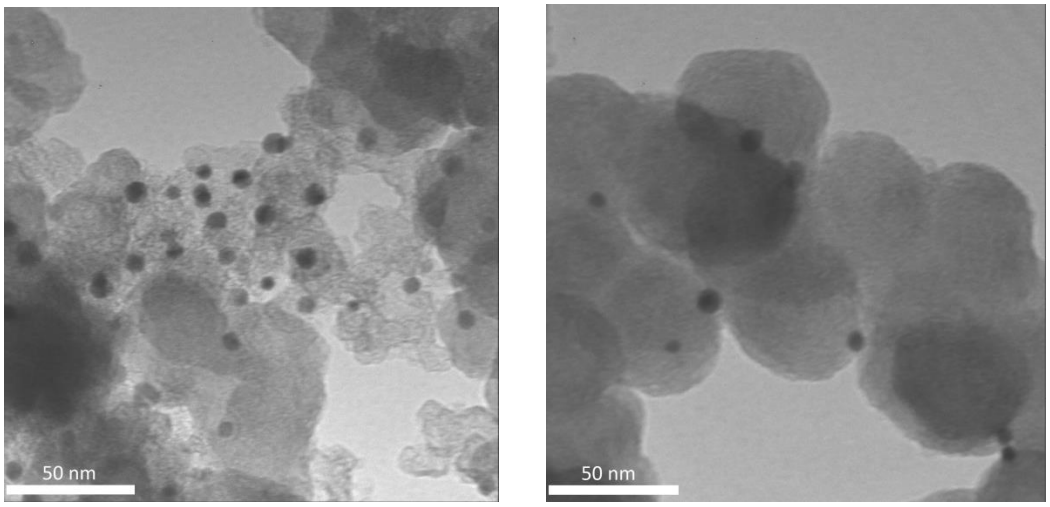

Figure 21. TEM images of Au-Fe_3O_3 nanoparticles deposited on carbon, treated with H_2SO_4 wash

It can be seen in the left image that the gold cluster has mostly dissociated from the iron-oxide domain, or conversely the iron-oxide domain was dissolved via the sulfuric acid. In the right image, the iron-oxide domain has grown to a much larger size with indefinite boundaries. Both of these results indicate the sulfuric acid reacted with the iron-oxide as expected, but with no useful control. The dimer-support product was then tested for benzyl alcohol oxidation catalysis. The GC analysis showed a range of unrecognized peaks that warranted further investigation. A GC-MS assay was used to analyze the catalysis experiment products, which confirmed that the products were not due to oxidation, but rather from reacting with residual sulfuric acid. These results demonstrated the sulfuric acid wash can etch away any hypothetical iron-oxide shell, but not with the desired precision needed for useful analysis.

Early on it was recognized that the size of the iron-oxide domain may not be appropriate for catalytic activity. A large Fe_3O_4 cluster can lead to steric hindrance, not allowing the Au nanoparticles to make efficient contact with the support material[18].

Stock solutions of Au-Fe_3O_4 heterodimers were synthesized with varying iron-oxide domain size from an average of 18 nm to an average of 11 nm, while keeping the size of the gold domain constant using Method A with no reflux (see Appendix). These sets of dimers were then used in all of the aforementioned catalytic trials and exposed to the same treatments such as support deposition and calcination, with none exhibiting substrate oxidation. These results suggest steric hindrance limiting surface accessibility was not a major concern.

Attempts were also made to vary the size of the gold domain as well. Pictured below are gold seeds synthesized via Method 1 with a size $\mu = 11.5$ nm and standard deviation $\sigma = 1.5$ nm (n=30). These gold seeds were then used to synthesize Au-Fe_3O_4 dimers, but each attempt resulted in a collection of gold and iron-oxide aggregates that did not follow the dimer template.

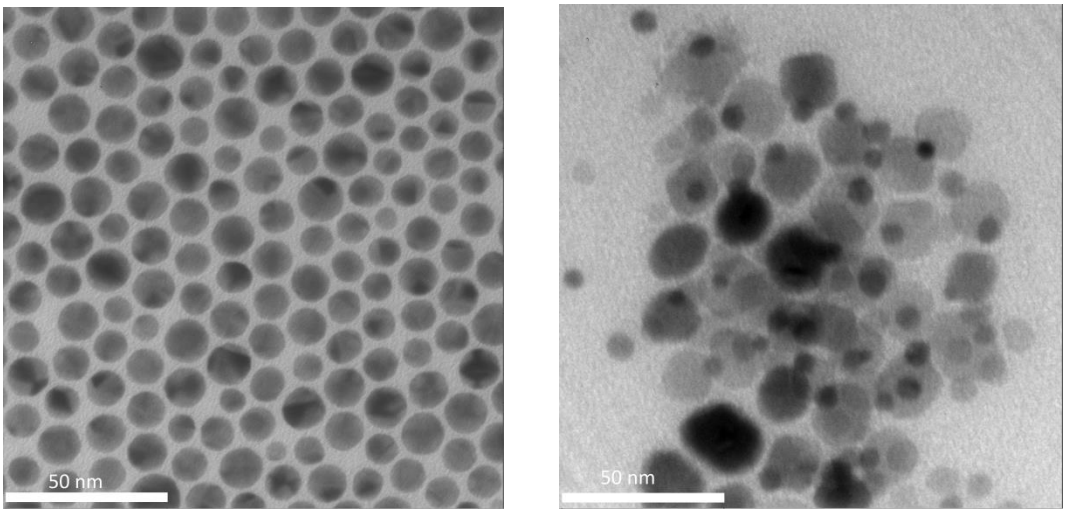

Figure 22. TEM images of Method 1 Au seeds (left) and Au-Fe_3O_4 nanoparticles (right)

Suitable Au-Fe_3O_4 heterodimers with discrete sizing and morphological control were only synthesized using gold seeds with a thiol capping reagent. Although both

Method 1 and Method 2 are published procedures using non-thiol based surfactants, the numerous trials giving undesired results emphasizes the stability the thiol ligand provides. However, it may be that the same thiol ligands are also creating an inaccessible surface environment, outcompeting both oxygen and substrate thus hindering the possibility of oxidation catalysis. Other unknown surfactants, present in the impure (70%) oleylamine reagent, may also create a similar effect.

Although organic alcohol oxidation catalysis was not achieved, the Au-Fe_3O_4 heterodimer system can now be examined from a different perspective. Future work should be concerned with dimer synthesis using gold nanoparticles that are stabilized via alternate surfactants, to help determine the surface effects thiol ligands have. This would also be a push toward more creative synthesis of the heterodimers using a broader screening of different ligands; it could also result in better size/morphological control. It would be of interest to find appropriate analytical methods to help characterize ligand exchange effectiveness. Additionally, other oxidants could be explored such as peroxide reagents which have a history of alcohol oxidation.

Conclusion

The system of Au-Fe_3O_4 heterodimer nanoparticles and their ability to catalyze organic alcohol oxidation has been studied. Different methods of dimer synthesis were explored, and it was determined that an adaption of a $Fe(acac)_3$ thermal decomposition onto Au seeds proved most stable and consistent. Catalytic experiment parameters were systemically altered to account for reaction temperature, time, substrate, and solvent

polarity. Ligand exchange methods were also probed to determine possible surface effects. The heterodimers were deposited on multiple supports with proven records of enhancing catalytic activity, and these composites were thermally treated due to additional surfactant concern. An effort was placed into changing gold and iron-oxide domain sizes, but the lack of synthetic capability at discrete sizing hindered these attempts. The Au-Fe_3O_4 system did not exhibit any oxidation catalysis of organic alcohols; future work on this system should be focused on synthesizing Au-Fe_3O_4 heterodimers that have weaker surfactants (without thiols) and better size control.

References

1) Corma, A.; Garcia, H. *Chem. Soc. Rev.* **2008,** *37,* 2096 – 2126.
2) Cortie, M. B.; Lingen, E. *Mater. Forum* **2002,** *26,* 1 – 14.
3) Daniel, M.-C.; Astruc, D. *Chem. Rev.* **2004,** *104,* 293 – 346.
4) Lin, F.; Doong, R. *J. Phys. Chem. C* **2011,** *115,* 6591 – 6598.
5) Wang, C.; Yin, H.; Dai, S.; Sun, S. *Chem. Mater.* **2010,** *22,* 3277 – 3282.
6) Prati, L.; Villa, A. *Catalysts* **2012,** *2,* 24 – 37.
7) Leyrey, J.; Vielhaber, B.; Zaki, M. I.; Shuxian, Z.; Weitkamp, J.; Knozinger, H. *Mater. Chem. Phys.* **1985,** *13,* 301 – 314.
8) Haruta, M. *Cattech* **2002,** *6,* 102 – 115.
9) Tamer, U.; Gundogdu, Y.; Boyaci, I. H.; Pekmez, K.; *J. Nanopart. Res.* **2010,** *12,* 1187 – 1196.
10) Sheng, Y.; Xue, J. *J. Colloid Interface Sci.* **2012,** *374,* 96 – 101.
11) Xie, J.; Zhang, F.; Aronova, M.; Zhu, L.; Quan, Q. et al. *ACS Nano* **2011,** *5,* 3043 – 3051.
12) Lee, Y.; Garcia, M. A.; Huls, N.; Sun, S. *Agnew. Chem. Int. Ed.* **2010,** *49,* 1271 – 1274.
13) Yin, H.; Wang, C.; Zhu, H.; Overbury, S. H.; Sun, S.; Dai, S. *Chem. Commun.* **2008,** *36,* 4357 – 4359.
14) Wu, B.; Zhang, H.; Chen, C.; Lin, S.; Zheng, N. *Nano Res.* **2009,** *2,* 975 – 983.
15) Stratakis, M.; Garcia, H. *Chem. Rev.* **2012,** *112,* 4469 – 4506.

16) George, C.; Dorfs, D.; Bertoni, G.; Falqui, A.; Genovese, A.; et al. *J. Am. Chem. Soc.* **2011,** *133,* 2205 – 2217.
17) Dong, A.; Ye, X.; Chen, J.; Kang, Y.; Gordon, T.; et al. *J. Am. Chem. Soc.* **2011,** *133,* 998 – 1006.
18) Wei, Y.; Bishop, K. J.; Kim, J.; Soh, S.; Grzybowski, B. A. *Agnew Chem. Int. Ed.* **2009,** *48,* 9477 – 9480.

Appendix

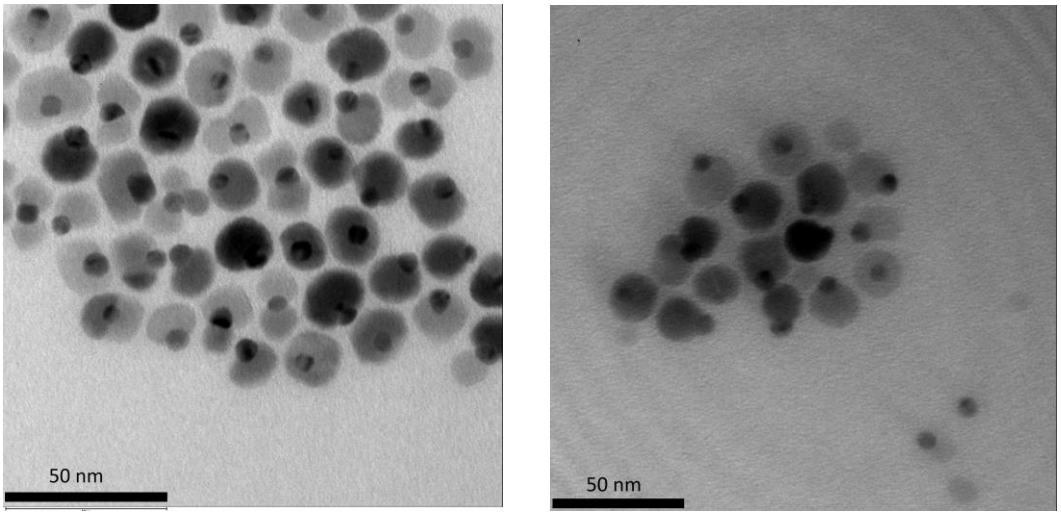

Figure 23. TEM Images of Au-Fe_3O_4 heterodimers with 11 nm (left) and 18 nm (right) iron-oxide domain

ACADEMIC VITA

Michael Schrenk

223 Delafield Road, Pittsburgh, PA 15215 / mgs5190@gmail.com

EDUCATION

The Pennsylvania State University, College of Engineering — University Park, PA

Schreyer Honors College — Graduation: May 2014

Bachelor of Science, Chemical Engineering

EXPERIENCE

Facilities Engineering Intern - Hess Corporation — Summer 2013

Undergraduate Chem. Research Assistant - REU Program — Summer 2012

Undergraduate Chem. Research Assistant - Schaak Group — 2011 – 2012

ACTIVITIES & LEADERSHIP

The Penn State IFC/Panhellenic Dance Marathon (THON)

ACACIA Fraternity

- •Founder/Co-Chair of Mentor Committee
- •Elected New Member Educator
- •Elected Programming Chair
- •Awarded Glenn Ream Scholarship

Baobob and Moringa Seed Oil Extractor Project, ENGR 493: Leadership Practicum

Member, American Institute of Chemical Engineers (AIChE)

SCHOLASTIC AWARDS

Conoco Scholarship in Engineering

Hollenbach Family Scholarship

Academic Excellence Scholarship

Pre-Eminence in Honors Education Scholarship

President’s Freshman Award